SQT



# Integrated and Spectral Energetics of the GLAS General Circulation Model

J. Tenenbaum

State University of New York

Purchase, New York 10577



[Submitted to Monthly Weather Review]


## ABSTRACT

Integrated and spectral error energetics of the GLAS General circulation model are compared with observations for periods in January 1975, 1976, and 1977. For two cases the model shows significant skill in predicting integrated energetics quantities out to two weeks, and for all three cases, the integrated monthly mean energetics show qualitative improvements over previous versions of the model in eddy kinetic energy and barotropic conversions. Fundamental difficulties remain with leakage of energy to the stratospheric level, particularly above strong initial jet streams associated in part with regions of steep terrain. The spectral error growth study represents the first comparison of general circulation model spectral energetics predictions with the corresponding observational spectra on a day by day basis. The major conclusion is that eddy kinetic energy can be correct while significant errors occur in the kinetic energy of wavenumber 3. Both the model and observations show evidence of single wavenumber dominance in eddy kinetic energy and the correlation of spectral kinetic and potential energy.

## 1. Introduction

Analysis of the generation, transport, and dissipation of energy represents one of the primary methods of studying geophysical fluid flows. Lorenz (1955) proposed subdividing atmospheric energy into kinetic and available potential forms and in turn subdividing these into zonal and eddy categories. Subsequent observational (Oort, 1964) and general circulation model (Manabe and Terpstra, 1974; Kasahara and Washington, 1971; and Somerville et al., 1974) studies have followed Lorenz's approach and will be referred to as integrated energetics analyses. Further subdivision in the spectral domain was suggested by Saltzman (1970) and followed by similar observational and model studies (Tenenbaum,1976; Wellck et al., 1971; Baker et al.,1978). One purpose of this paper is to examine both the integrated and spectral energetics of the current Goddard Laboratory for Atmospheric Sciences (GLAS) model.

The most direct test of a model over a period of several days is the quality of the prediction of standard meteorological variables. Comparisons are made either in terms of synoptic discussions (generation and deepening of lows, etc.), root-mean-square errors, or the related idea of skill scores (Tewles and Wobus, 1954; Atlas, 1979). One knows theoretically that these approaches should give an essentially random result at a predictability limit of the order of 14 d and in practice do so in about 5 d (Lorenz, 1967).

To extract further information in spite of these limits, one employs various space and time averages applied to both meteorological variables and energetics quantities. These averaged quantities may show skill for periods approaching or exceeding the predictability limit; indeed current general circulation models are characterized by quite reasonable model "climates." One of the commonly held intuitions is that low wavenumber spectral quantities qualify as "averaged" quantities. A second purpose of this paper is to examine that assumption and to display circumstances where it is more or less valid.

In this paper we will follow Saltzman in employing one-dimensional wavenumber spectra consisting of Fourier transforms around latitude circles. An alternate analysis in terms of two-dimensional spatial spectra was suggested by Baer (1972) and is related to many spectral models. A subsequent paper will present two-dimensional results (Tenenbaum, to be published).

The wavenumber domain spectra presented here form one member of a trio of approaches concerning atmospheric wave phenomena. Frequency domain studies deal with spectral analyses of variables in that domain while space-time analyses take both approaches simultaneously. These approaches are complementary, with the wavenumber approach allowing us to study the time dependence of energetics and spectral quantities. In particular, we can study the growth of errors toward the predictability limits for a variety of synoptic situations. It is the study of these

synoptic dependences which form the third purpose of this paper.

In this paper we do not separate transient and stationary effects. As we shall subsequently see the intense stationary jet stream anchored east of Japan tends to dominate wavenumber 3 results. While time means could be subtracted from each of our independent variables, we are hesistant to do so until we have a better sense of the interannual variability. A final and distinctive feature of this study is the use of model spectra in comparison with the spectra derived from observations for corresponding times. Studies of model spectra and of observational spectra have been separately performed; no spectral energetics study for the corresponding times has yet been published.

## 2. Model and methods

The GLAS general circulation model represents the third in a series of models. The original Mintz-Arakawa model (Arakawa, 1972) was a 3-level model incorporating Arakawa's energy and enstrophy conserving difference scheme. The second in the series, the Goddard Institute for Space Studies (GISS) model was a combination of Arakawa's approach with modified convection and radiation schemes (Somerville et al., 1974). Subsequent papers have dealt with its spectral properties (Tenenbaum, 1976), synoptic performance (Druyan et al., 1974), seasonal behavior (Stone et al., 1977), and behavior over semi-arid regions (Charney et al., 1977).

The GLAS model differs from the GISS model primarily in the application of a Shapiro filter to the dependent variables and an improved radiation routine. Specific changes include (Halem et al., 1978): (1) improved long wave radiation formulation, (2) increased radiative process time step, (3) prognostic rather than prescribed soil moisture along with other hydrological changes, (4) smoothly varying sea-surface temperature changes, (5) changed surface albedo, (6) coarsening of zonal resolution in 5 bands towards the poles, and increased advective time step (10 min) with decreased smoothing near the poles.

The integrated energetics quantities are calculated according to

the formulas given in Oort (1964) for the mean zonally averaged kinetic energy, $K_M$, and the zonally averaged eddy kinetic energy, $K_E$ (i.e. the zonal average of the deviations from the zonal mean). Using Oort's nomenclature, both quantities are calculated in the space domain.

The spectral analysis methods are taken from Saltzman (1970) and are described in further detail in Tenenbaum (1976). One-dimensional Fourier spectra are calculated around each latitude circle at each of the nine levels every 12 h. Tropospheric results represent the average of the lowest 8 levels (centers from 175 mb to 945 mb) over the entire Northern Hemisphere. Because of problems with National Meteorological Center (NMC) observational results at 1200 GMT prior to April 1975 (Spar et al., 1976), all graphs are from 0000 GMT data. No significant differences appeared when comparisons also included valid 1200 GMT data. The three periods discussed in this paper represent model predictions initialized at 0000 GMT 1 January 1975, 1976, and 1977. The climate averages represent 1 month averages from 0000 GMT 1 January through 1200 GMT on 31 January. The time dependent graphs run over the periods noted.

## 3. Synoptic energetics summary

We present in this section a synoptic summary of the periods covered, in both conventional and energetics terms. Tropospheric results refer to the Northern Hemisphere troposphere, consisting of

levels 2 through 9 of the GLAS model and extending from 120 mb to the surface. Integrated energetics diagrams have been presented by Oort (1964) for observations and each of the major modeling groups for the general circulation models (Manabe et al., 1970; Wellck et al., 1971; Stone et al., 1977). The typical time dependent behavior (Baker et al., 1978; see also Fig. 6 below) shows two primary features: $K_M$ and $K_E$ tend to be anti-correlated and $K_E$ typically varies between 5 and $9 \times 10^5$ $J/m^2$.

Spectral energetics distributions have been similarly documented (Tenenbaum, 1976) and show two characteristic features in the eddy kinetic energy spectrum. First, the bulk of the energy is in wavenumbers 1 through 5 and, second, there is a characteristic log-linear falloff for wavenumbers above 8. The relationship of the latter to theories of turbulence has been extensively discussed in the literature (Charney, 1971).

Since our subsequent concerns deal with the distribution and redistribution of eddy kinetic energy among the individual wave numbers, it is instructive to match the synoptic maps with the spectra. Fig. 1 shows the 200 mb map for 0000 GMT 1 January 1977. To a good approximation the bulk of eddy kinetic energy is located at this level (Fig. 15 in Tenenbaum, 1976 and subsequent figures below). Table 1 presents the corresponding energy spectra.

Examination of the map shows a very characteristic subtropical jet

south of Japan. This jet appears in conjunction with lesser jets centered over the Western Atlantic and Saudi Arabia and is consistent with the quasi-stationary winter average wave pattern found by Krishnamurti (1961). For January 1976 (not shown) we have a strong polar jet centered over Norway and a much weaker subtropical jet in that sector. These jets provide the dominant contributions to tropospheric $K_E$, and especially to the spectral subcomponents of $K_E$, given by $K_n$. The model's ability to predict the growth and decay of these jets will determine its ability to predict $K_E$ and $K_n$.

We can correlate the jet stream behavior with the spectral analysis by comparing the 200 mb charts with the individual $K_n$ given in Table 1. For 1977 we see an initially dominant n = 2 pattern characterized by the intense Japan jet matched with a North American jet not quite 180° away. By 0000 GMT 7 January (Fig. 2) we see a flip to dominance by n = 1 and 3 in Table 1 and a corresponding change in the jet stream pattern. The Atlantic portion of the North American jet has been cut off and a Saudi Arabian jet has grown to above 150 KT (77 m/s). Two of the three peaks contributing to the n = 3 component are easily visible while the n = 1 component arises from the less obvious polar asymmetry. In more conventional terms the first half of 1977 was characterized as follows (see Wagner, 1977): A strong blocking ridge was located just off western North America. This ridge weakened during the second week simultaneous with the growth a strong trough in the Alantic. This last effect occurred in conjunction with an intense stratospheric warming whose effects include a significant zonal flow over Hudson Bay (Fig. 3).

## 4. Integrated energetics

Probably the most commonly seen failure of general circulation models has been the deficit of $K_E$. Most early models had this problem and while some improvement was noted in the GISS model (Somerville et al., 1974) the exact situation is still puzzling. Why should a change in resolution at scales far removed from the bulk of $K_E$ produce the partial improvement (Manabe, 1970)?

A corollary to the weak $K_E$ has been its diffuse distribution. Figs. 4 and 5 show observation, the GISS model distribution, and the GLAS model distribution of $K_E$ plotted as a zonal average versus pressure and latitude. Even more striking is the conversion of $K_E$ to $K_M$ which has a characteristic dipole pattern in the observations and lacks it in the previous models (Fig. 5). Corresponding results were noted for the National Center for Atmospheric Research (NCAR) model (Baker et al., 1977, Fig. 9). The change in Figs. 4 and 5 is substantial, since the negative portion of the dipole is now better located and of appropriate intensity. Some combination of the radiative improvement and the decreased smoothing has produced a significant change in those distributions, both in the integrated energetics and amongst the conversions.

## 5. Spatial energetics

Our central results concern the interplay of the eddy kinetic energy and its spectral subcomponents. Fig. 6 shows the observational and model values of $K_M$ and $K_E$ for the first two weeks of each time period. For two relatively different synoptic situations the model tracks the atmosphere's $K_E$ out to a period approaching 12 d. The agreement is not so much one of quantitative precision as trend following with a probability that is visibly non-random. Note that for the $K_E$ rise in January 1977 there appears to be a 1 d lag. A reasonable interpretation is the existence of predictive skill in an averaged quantity out to the predictability limits.

While these two cases seem stronger than a random correlation, the third case shows far less success. For January 1976 the model seems unable to maintain or generate the $K_E$ needed to follow the atmosphere's rise. Upon examining the energy flows more closely, we discover several significant phenomena. Consider first tropospheric $K_M$. The cases consist of one low $K_M$ state (January 1976), one average $K_M$ state (January 1975), and one strikingly high $K_M$ state (January 1977). The latter case is unusual and was sustained at or near this high value throughout the 2 weeks. The model, in contrast, for the three cases has only one pattern: monotonic growth. Some of the success of January 1977 is clearly due to the atmosphere's happening to match this built in bias of the model.

An even stronger anomaly appears in the time displays of stratospheric $K_M$ shown in Fig. 7. There appears to be a ubiquitous tendency for zonal energy to collect in the model's topmost layer, with significant excess energy present in the model's one stratospheric level in periods of 4 to 6 d. Since there are no significant dissipative mechanisms at that level, the excess energy appears to remain trapped there, functioning as a resevoir of $K_M$ and $K_E$, but distorting the behavior of the individual wavenumbers. In another paper (Kalnay-Rivas and Tenenbaum, 1980) we examine this effect over the first 48 h and show the existence of major oscillations with a period of about 24 h. As discussed there, these oscillations do seem to be attenuated by enhanced vertical resolution near the tropopause.

The monotonic rise to unrealistically high levels also appears in stratospheric values of $K_E$ (Fig. 8). The 1976 case gains eddy kinetic energy in the model stratosphere much faster than the other two years, and at the same time that the troposphere is rapidly losing energy. The failure in this case is due to the model's inability to correctly maintain a strong polar jet stream over Norway, resulting perhaps from the smoothing at higher latitudes.

Perhaps our most suggestive result concerns the longitudinal dependence of the stratospheric leakage. In all three cases we see what appears to be vertical transport of energy upward from the initial jets. Fig. 9 shows a time series of meridional cross sections of the zonal wind at 90° E, the entry region of the subtropical jet centered south of

Japan. The observed data show moderate fluctuations while the model shows a conversion from an "o" pattern to a "u" pattern with a characteristic time of 4 to 8 d. This same behavior occurred above all jets for all three cases and seems to be the antecedent of the "u" shaped average pattern characteristic of most models. (Fig. 4 above; Miyakoda et al., 1972, Fig. 2).

An alternate way of examining this phenomena is shown in Fig. 10 which presents the time series of the zonal wind at the stratospheric level. The observational series shows moderate fluctuations of regions with winds greater than 30 m/s centered above Norway and Japan. No values exceed 40 m/s. In strong contrast, the model's time series shows an inkblot-like rise above Japan which grows to speeds exceeding 60 m/s and which propagates downstream to the Aleutians (9 January) and the Yukon (13 January). The vertical leakage above the strong initial jets occurred in all three years though only in the case illustrated (January 1975) did the energy propagate downstream. For January 1976 and 1977 the pool of energy remained above its origin (Norway and Japan, respectively).

This behavior seems very striking, and may provide a clue to the cold polar stratosphere phenomena seen in most general circulation model winter simulations. Excess kinetic energy is reaching the mid-latitude stratosphere, and consistent with the thermal wind relation, erroneously modifying the polar stratosphere.

## 6. Spectral energetics

In striking contrast to the successful $K_E$ predictions for January 1975 and January 1977 is the behavior of wavenumber 3. One can isolate the one or two dominant wavenumbers with little difficulty. Fig. 11 shows the time history of $K_1$ and $K_3$ for these two years. (These two wavenumbers are 100% higher than the peak value of all other wavenumbers). In spite of the noisy signal, one sees a much more discrepant behavior with gross errors in wavenumber 3 at times when the summed $K_E$'s remain correct.

In terms of Saltzman's spectral energetics analysis one can imagine two possibilities: (1) erroneous transports in or out of the Northern Hemisphere troposphere, or (2) erroneous conversions from zonal potential or kinetic energy. As is inevitable, the sorting out of cause and effect will probably be difficult.

As shown in Fig. 10 the erroneous stratospheric energy seems to be billowing up above the quasi-permanent jets. This transport shows up very strongly in both $K_M$ (Fig. 7) and $K_E$ (Fig. 8). As a result wavenumber 3 has been deprived of the major portion of the energy needed to maintain the observed values of the subtropical jets in their characteristic standing wave pattern. Wavenumber 1, which is dominated by a combination of the polar asymmetry and hemispheric contrasts, is less affected.

The spectral analysis approach is useful in pinpointing the location of other difficulties. As shown in Fig. 11, the model's $K_3$ for January 1977 does very poorly starting about 6 January of the run. Examination of the various conversions away from the locations of the leakage to the stratosphere shows a clear example of how the spectral conversion can pin down the cause of this discrepancy in a causal sense. Fig. 12 shows the latitude-pressure distribution of $K_3$, and the conversions $C(K_3,K_M)$ and $C(K_3,K_n)$ [Saltzman's M and L, respectively] for 0000 GMT on 1 January 1977 and 5 January 1977, just before the start of the discrepancy. While the model has correctly predicted the qualitative and rough quantitative behavior of $K_3$, the conversions are already qualitatively incorrect. $C(K_3,K_M)$ is erroneously draining the model's K south of the sub-tropical jet while $C(K_3,K_n)$ is building $K_3$ at what will be the location of the statospheric warming 4 d later. The model displaces this conversion to coincide with the jet itself.

One other commonly suggested difficulty does not appear. The phases of the energy in individual wavenumbers appear to agree when the wavenumber magnitudes themselves agree. Fig. 13 shows the phase diagrams corresponding to Fig. 6 for January 1977. Both model and observation appear matched in phase until 7 January

The spectral analysis techniques seem useful in on other way. Fifty percent of the amplitude of the stratospheric warming of 11

January appears in observational wavenumber 3 analyses at approximately 70°N. The model missed this warming, though in fairness, this was a feature not appearing until 10 d into the forecast. The presence of a very strong observational signal in wavenumber 3, and dominantly there, suggests a potential analytic tool for following up this phenomena.

Two other general conclusions emerge from the spectral results. The first, not previously noted, concerns the behavior of the individual wavenumber $K_n$'s. One appears to have a phenomena best described as single wavenumber dominance. In Fig. 14 we show 30 d series of the first six observational $K_n$. On a purely chance basis there appears to be far less than the expected amount of overlaps between the individual peaks. The relation of this result to some of Charney's work on oscillations between climate states is not clear.

The second, noted by Tsay and Kao (1978) and others, is the very close tracking of the kinetic and potential eddy terms. As shown in Fig. 15, the effect is clearly present for n = 1 and 3 and absent for n = 2. The other years show similar effects. It contrasts with the negative correlation shown by $K_M$ and $K_E$ in Fig. 6, a result which one tends to expect on the basis of energy conservation.

## 7. Some problem areas for spectral energetics

The insights provided by the spectral energetics approach have been presented above as techniques for localising model failure at times when integrated eddy quantities are showing agreement. There remain, however, several problem areas which require further study to increase one's confidence in the analytic method, or the behavior of the atmosphere, or both. These areas include the issues of atmospheric cause and effect, the consistency of the conversions, and the calculation of vertical velocity dependent quantities.

Tsay and Kao (1978) and Kao and Chi (1978) have made detailed studies for the period 1 December 1975 through 29 February 1976 in the wavenumber-time and wavenumber-frequency domains, respectively. Working with the observations, and predominantly at 500 mb between 30°N and 60°N, they attempt to trace the growth and decay of waves in the long (n = 1 to 3) and synoptic (n = 4 to 8) scales. They conclude that "the growth and decay of the kinetic energy of the long and synoptic scale waves are primarily controlled by the transport of kinetic energy to and from the waves through non-linear wave interactions while the contribution to the kinetic energy conversion tends to balance the effects of the Reynolds and frictional stresses." (Kao and Chi, 1978, abstract).

Their paper contains several well documented examples of the

correlation of changes in individual $K_n$ with the non-linear conversion term. We question, however, whether such data demonstrates causation or simply correlation. Their data tends to show changes in conversions occurring at similar times as the change in the corresponding energy, rather than clearly preceding it as in Fig. 12 above.

Beyond this issue, more general questions remain concerning the consistency of results obtained by applying Saltzman's spectral energetics analysis. The equations themselves are not in question but rather the quality of results from their application to either model or observational data. Saltzman's equations provide a closed system with respect to conversions into and out of individual $K_n$. The algebriac sum of the conversions integrated over an appropriate space and time period should equal the secular change in the corresponding $K_n$. While such a result requires assuming the validity of dissipation calculations, $D_n$, the lack of agreement gives us some sense of our overall confidence in the results. Because of the unavailabity of independent data for $D_n$, Saltzman had to calculate it only as a residual.

The results are not encouraging. Table 2 presents this type of calculation for a sampling of model and observational runs. For most cases the sign of the change is incorrect and in some cases the individual $K_n$ should have been driven solidly and unphysically negative. Three posible explanations seem most likely: errors in $C_n$, $D_n$, and vertical transports. The conversion $C_n$, and to a lesser extent some

others, depend on the vertical velocity, $\omega$. For the observations this is a notoriously difficult quantity to evaluate. $D_n$ is a parameterized quantity whose physical basis is known in broad terms but whose detailed quantitative evaluation requires confidence in surface winds and boundary layer effects. Vertical transports are clearly a problem for the model and may be a problem for the observations.

We will examine the vertical velocity problem in detail in a subsequent paper (Tenenbaum and Reddi, to be published). Our preliminary results show that alternate formulations for $\omega$ (changing from mass convergence to iterative solution of the diagnostic omega equation can yield major changes in long- and synoptic scale values of C and extensive smoothing of the higher wavenumbers.

## 8. Conclusions and future directions

We have studied the model's medium range skill and climatology using various possible integrated quantities. Our major conclusions are as follows:

(1) The model can show medium range skill in an integrated quantity, K , the Northern Hemisphere tropospheric eddy kinetic energy, out to the predicability limit of two weeks in two of three randomly chosen cases.

(2) The model climatology is significantly improved over previous versions in terms of the monthly time-mean energetics. This effect is most striking as sharper gradients in the zonal average of $K_E$ and the characteristic dipole behavior of the barotropic conversion terms.

(3) The model retains a bias in accumulating energy in the topmost, stratospheric, level. The accumulation appears predominantly above the strong initial jets and downstream of the location of the quasi-permanent jets associated with steep orography. The tropospheric $K_M$ also appears to grow to unreasonably large values.

(4) In the presence of this stratospheric leakage, wavenumber 3 appears questionable in the role of an integrated energetics quantity; $K_E$ can show agreement while wavenumber 3 is erroneous. An expanded version of Saltzman's spectral analysis (including transports) does provide a useful tool in showing cause and effect relations for where the model is failing to match significant energy flow in the atmosphere.

These approaches must be used with care since Tsay and Kao's studies seem to show more correlation than causation. The spectral coefficients do show interesting results in terms of single wavenumber dominance (not previously noted) and kinetic energy tracking of potential energy (noted by Tsay and Kao).

A number of future directions are indicated. More synoptic cases should be studied, both randomly chosen, and specially chosen to explore the factors cited above ($K_M$ high or low, fast or slow propagation to the stratosphere, jet strong and well or poorly defined). A model with better resolution near the tropopause is needed which probably implies a shift to uneven spacing in pressure. If the stratospheric leakage is the result of erroneous waves induced by steep terrain, we may need to improve the conservation properties of the model in these regions (see Arakawa and Lamb, 1977). Alternatively, if the problem is erroneous jet stream or vertical velocity initialization, we may need to examine more complex initialization schemes to reduce the initial shock. In view of the presence of strong oscillations and strong leakage in all three cases, both effects are most likely present.

Acknowledgements. I would like to thank Drs. M. Halem, J. Shukla, W. Baker, and Y. Sud at the Goddard Laboratory for Atmospheric Sciences and Professors R. Lindzen and J. Spar for helpful comments throughout this work; M. Johnson, D. Leighton, and J. Lengel for programming assistance; and G. Federico, R. Rabinowitz, and B. Sganga for graphics assistance. This work was supported by National Aeronautics and Space Administration Grant NSG-5077.

## References


Arakawa, A., 1972: Design of the UCLA atmospheric general circulation model. Tech. Rept. No. 7, Dept. of Meteorology, University of California at Los Angeles.

----, and V. R. Lamb, 1977: Computational design of the basic dynamical processes of the UCLA general circulation model. Methods in Computational Physics, Vol. 17, General Circulation Models of the Atmosphere, J. Chang, Ed., Academic Press, 173-265.

Atlas, R., M. Halem and M. Ghil, 1979: Subjective evaluation of the combined influence of satellite temperature sounding data and increased model resolution of numerical weather forecasting. Proceedings of the Fourth Conference on Numerical Weather Prediction, Silver Spring, Md. Boston, Amer. Meteror. Soc.

Baer, F., 1972: An alternate scale representation of atmospheric energy spectra. J. Atmos. Sci., 29, 649-664.

Baker, W. E., E. C. Kung, and R. C. J. Somerville, 1977: Energetics diagnosis of the NCAR general circulation model. Mon. Wea. Rev., 105, 1384-1401.

----, ----, and ----, 1978: An energetics analysis of forecast experiments with the NCAR general circulation model. Mon. Wea. Rev., 106, 311-323.

Charney, J. G., 1971: Geostrophic turbulence. J. Atmos. Sci., 28, 1087-1095.

----, P. H. Stone, and W. J. Quirk, 1975: Drought in the Sahara:

a biogeophysical feedback mechanism. Science, 187, 435-436.

Druyan, L. M., R. C. J. Somerville and W. J. Quirk, 1975: Extended range forecasts with the GISS model of the global atmosphere. Mon. Wea. Rev., 103, 779-795.

Halem, M., J. Shukla, Y. Mintz, M. L. Wu, R. Godbole, G. Herman and Y. Sud, 1978: Comparisons of observed seasonal climate features with a winter and summer numerical simulation produced with the GLAS general circulation model. Proceedings of the JOC Study Conference on Climate Models held on April 3-7, 1978 in Washington, D.C.

Kalnay-Rivas, E., and J. Tenenbaum, 1980: Initial oscillations at upper levels of the GLAS general circulation model. (to be submitted to Mon. Wea. Rev.)

Kao, S. K., and C. N. Chi, 1978: Mechanism for the growth and decay of long- and synoptic-scale waves in the mid-troposphere. J. Atmos. Sci., 35, 1375-1387.

Kasahara, A., and W. M. Washington, 1967: NCAR global general circulation model of the atmosphere. Mon. Wea. Rev., 95, 389-402.

Krishnamurti, T. N., 1961: The subtropical jet stream of winter. J. Meteorol., 18, 172-191.

Lorenz, E. N., 1955: Available potential energy and the maintenance of the general circulation. Tellus, 7, 157-167.

----, 1967: The nature and theory of the general circulation of the atmosphere. WMO Publ. 218-TP-115, Geneva, 161 pp.

Manabe, S. J., J. Smagorinsky, J. L. Holloway, Jr. and H. M. Stone, 1970:

Simulated climatology of a general circulation model with a hydrologic cycle. III. Effects of increased horizontal computational resolution. Mon. Wea. Rev., 98, 175-212.

----, and T. B. Terpstra, 1974: The effects of mountains on the general circulation of the atmosphere as identified by numerical experiments. J. Atmos. Sci., 31, 3-42.

Miyakoda, G. D. Hembree, R. F. Strickler and I. Shulman, 1972: Cumulative results of extended forecast experiments I. Model performance for winter cases. Mon. Wea. Rev., 100, 836-855.

Oort, A. H., 1964: On estimates of the atmospheric energy cycle. Mon. Wea. Rev., 92, 483-493.

Peixoto, J. P., and A. H. Oort, 1974: The annual distribution of atmospheric energy on a planetary scale. J. Geophys. Rsch., 79, 2149-2159.

Saltzman, B., 1970: Large scale atmospheric energetics in the wavenumber domain. Rev. Geophys. Space Phys., 8, 289-302.

Somerville, R. C. J., P. H. Stone, M. Halem, J. E. Hansen, J. S. Hogan, L. M. Druyan, G. Russell, A. A. Lacis, W. J. Quirk and J. Tenenbaum, 1974: The GISS model of the global atmosphere. J. Atmos. Sci., 31, 84-117.

Spar, J., R. Atlas and E. Kuo, 1976: Monthly mean forecasts with the GISS model. Mon. Wea. Rev., 104, 1215-1242.

Stone, P. H., S. Chow and W. J. Quirk, 1977: The July climate and a comparison of the January and July climates simulated by the GISS general circulation model. Mon. Wea. Rev., 105, 170-194.

Tenenbaum, J., 1976: Spectral and spatial energetics of the GISS model atmosphere. Mon. Wea. Rev., 104, 15-30.

Tenenbaum, J., and M. Reddi, to be submitted to Mon. Wea. Rev..

Tewles, S. Jr, and H. B. Wobus, 1954: Verification of prognostic charts. Bull. Amer. Meteor. Soc., 35, 455-463.

Tsay, C-Y., and S.-K. Kao, 1978: Linear and nonlinear contributions to the growth and decay of the large-scale atmospheric waves and jet stream. Tellus, 30, 1-14.

Wagner, A. J., 1977: Weather and circulation of January 1977. Mon. Wea. Rev. 10, 553-560.

Wellck, R. E., A. Kasahara, W. M. Washington and G. De Santo, 1971: Effect of horizontal resolution in a finite difference model of the general circulation. Mon. Wea. Rev., 99, 673-683.

## Table Captions

Table 1. $K_M$, $K_n$, and $K_E$ at 0000 GMT on indicated dates for observations and model predictions. Data are for the Northern Hemisphere troposphere (120 mb to 1000 mb). Units: $10^5$ J / $m^2$.

Table 2. Changes in $K_3$ for observations and model predictions. Upper section shows secular change over the 2 day period indicated. Lower section gives corresponding change in $K_3$ implied by the conversions averaged over the corresponding 2 day period. The first two conversions feed energy to $K_3$, the last two drain energy from $K_3$. These results are quite typical. Data is for the Northern Hemisphere troposphere (120 mb to 100C mb).

Table 1. $K_M$, $K_n$, and $K_E$.

| | observations | | | | | model | |
|---|---|---|---|---|---|---|---|
| K | 1 Jan. 1975 | 1 Jan. 1976 | 1 Jan. 1977 | 7 Jan. 1977 | 11 Jan. 1977 | 7 Jan. 1977 | 11 Jan. 1977 |
| M | 7.54 | 6.76 | 9.89 | 8.73 | 9.12 | 9.58 | 10.37 |
| 1 | 1.72 | 1.58 | 1.05 | 2.18 | 1.14 | 1.64 | 0.83 |
| 2 | 0.38 | 0.70 | 1.77 | 1.11 | 0.92 | 0.62 | 0.63 |
| 3 | 1.64 | 1.21 | 0.99 | 1.75 | 1.92 | 1.06 | 0.71 |
| 4 | 0.57 | 0.52 | 0.57 | 0.98 | 0.81 | 0.67 | 1.17 |
| 5 | 0.52 | 0.39 | 0.42 | 0.28 | 0.96 | 0.97 | 0.38 |
| 6 | 0.64 | 0.33 | 0.45 | 0.46 | 0.46 | 0.47 | 0.25 |
| 7 | 0.19 | 0.96 | 0.26 | 0.39 | 0.21 | 0.47 | 0.27 |
| 8 | 0.49 | 0.22 | 0.12 | 0.18 | 0.17 | 0.42 | 0.41 |
| 9 | 0.19 | 0.42 | 0.14 | 0.19 | 0.49 | 0.33 | 0.47 |
| 10 | 0.12 | 0.35 | 0.16 | 0.11 | 0.20 | 0.14 | 0.19 |
| 11 | 0.17 | 0.18 | 0.11 | 0.30 | 0.20 | 0.10 | 0.10 |
| 12 | 0.07 | 0.05 | 0.09 | 0.15 | 0.14 | 0.07 | 0.19 |
| 13 | 0.06 | 0.05 | 0.03 | 0.04 | 0.04 | 0.12 | 0.10 |
| 14 | 0.04 | 0.03 | 0.03 | 0.05 | 0.05 | 0.09 | 0.08 |
| 15 | 0.04 | 0.03 | 0.03 | 0.02 | 0.05 | 0.07 | 0.02 |
| E | 6.97 | 7.22 | 6.40 | 8.35 | 7.91 | 7.41 | 6.10 |

Table 2. $K_3$ conversion balance

| | observation | model |
|---|---|---|
| $K_3$ | ($10^5$ J / $m^2$) | ($10^5$ J / $m^2$) |
| 0000 GMT 8 Jan. 1977 | 1.5 | 1.5 |
| 0000 GMT 6 Jan. 1977 | 0.6 | 1.5 |
| $K_3$ change | +0.9 | 0.0 |
| average conversions | (W / $m^2$) | (W / $m^2$) |
| $P_3$ to $K_3$ | -0.3 | 0.0 |
| $K_n$ to $K_3$ | 0.0 | -0.5 |
| $D_3$ | 0.1 | 0.1 |
| $K_3$ to $K_M$ | 0.2 | 0.4 |
| net conversion | -0.6 | -0.8 |
| | ($10^5$ J / $m^2$) | ($10^5$ J / $m^2$) |
| implied $K_3$ change | -1.0 | -1.4 |

## Figure Captions

Fig. 1. Constant pressure chart at 200 mb for 0000 GMT 1 January 1977. Contodr interval is 120 m.

Fig. 2. Constant pressure chart at 200 mb for 0000 GMT 7 January 1977. Contour interval is 120 m.

Fig. 3. Constant pressure chart at 200 mb for 0000 GMT 11 January 1977. Contour interval is 120 m.

Fig. 4. Monthly mean of eddy kinetic energy, $K_E$. (a) Climatological average for January from Peixoto and Oort (1974). (b) GISS model from Tenenbaum (1976). (c) NMC observations for January 1975. (d) GLAS model prediction for January 1975.

Fig. 5. Monthly mean of the conversion $K_E$ to $K_M$. (a) Climatological average for January from Peixoto and Oort (1974). (b) GISS model from Tenenbaum (1976). (c) NMC observations for January 1975. (d) GLAS model prediction for January 1975.

Fig. 6. Time history of tropospheric mean kinetic energy, $K_M$, and eddy kinetic energy, $K_E$, for the first two weeks of each case. (a) January 1975. (b) January 1976. (c) January 1977.

Units: $10^5$ J / $m^2$.

Fig. 7. Time history of mean kinetic energy, $K_M$, for the stratospheric level (10 mb to 120 mb). Model data for all three cases and observational data for January 1975. The observational data for January 1976 and 1977 were similar to 1975. Units: $10^5$ J / $m^2$ bar.

Fig. 8 Time history of eddy kinetic energy, $K_E$, for the stratospheric level (10 mb to 120 mb). Model data for all three cases and observational data for January 1975. The observational data for January 1976 and 1977 were similar to 1975. Units: $10^5$ J / $m^2$ bar.

Fig. 9. Jet stream cross sections of the zonal wind at longitude 90°E . (a) Observations. (b) Model predictions. Data are for 0000 GMT on 1, 5, 9, and 13 January 1975, respectively. Regions above 30 m / s are shaded.

Fig. 10. Surface display of the zonal wind at the stratospheric level (10 mb to 120 mb). (a) Observations. (b) Model predictions. Data are for 0000 GMT on 1, 5, 9, and 13 January 1975, respectively. Regions above 30 m / s are shaded.

Fig. 11. Time history of eddy kinetic energy of wavenumbers 1 and 3

(a) January 1975. (b) January 1977. Units: $10^5$ J / $m^2$.

Fig. 12. Pressure-latitude display of $K_3$, the conversion $K_3$ to $K_M$, and the conversion $K_n$ to $K_3$. (a) The initial state at 0000 GMT 1 January 1975. (b) The situation at 0000 GMT 5 January 1975 just before $K_3$ starts to diverge between model and observation. (c) The model prediction at 0000 GMT 5 Janaury 1975.

Fig. 13. Polar diagram of $K_3$ magnitude and phase for observations and model. Data are the layer average from 220 mb to 330 mb (level 3 of the GLAS model) at $30^{\circ}$N. This combination of pressure and latitude is near the peak of the $K_3$ distribution. Labels indicate days after initial state. (a) January 1975. (b) January 1977. Units (radial): $10^5$ J / $m^2$.

Fig. 14. Time history of the individual $K_n$ for n = 1 to 6 for Janaury 1975. (a) Observations. (b) Model. Units: $10^5$ J / $m^2$.

Fig. 15. Time history of the available potential energy, $P_n$, and the eddy kinetic energy, $K_n$, for n = 1 to 3 for observational and model data for Janaury 1975. Units: $10^5$ J / $m^2$.

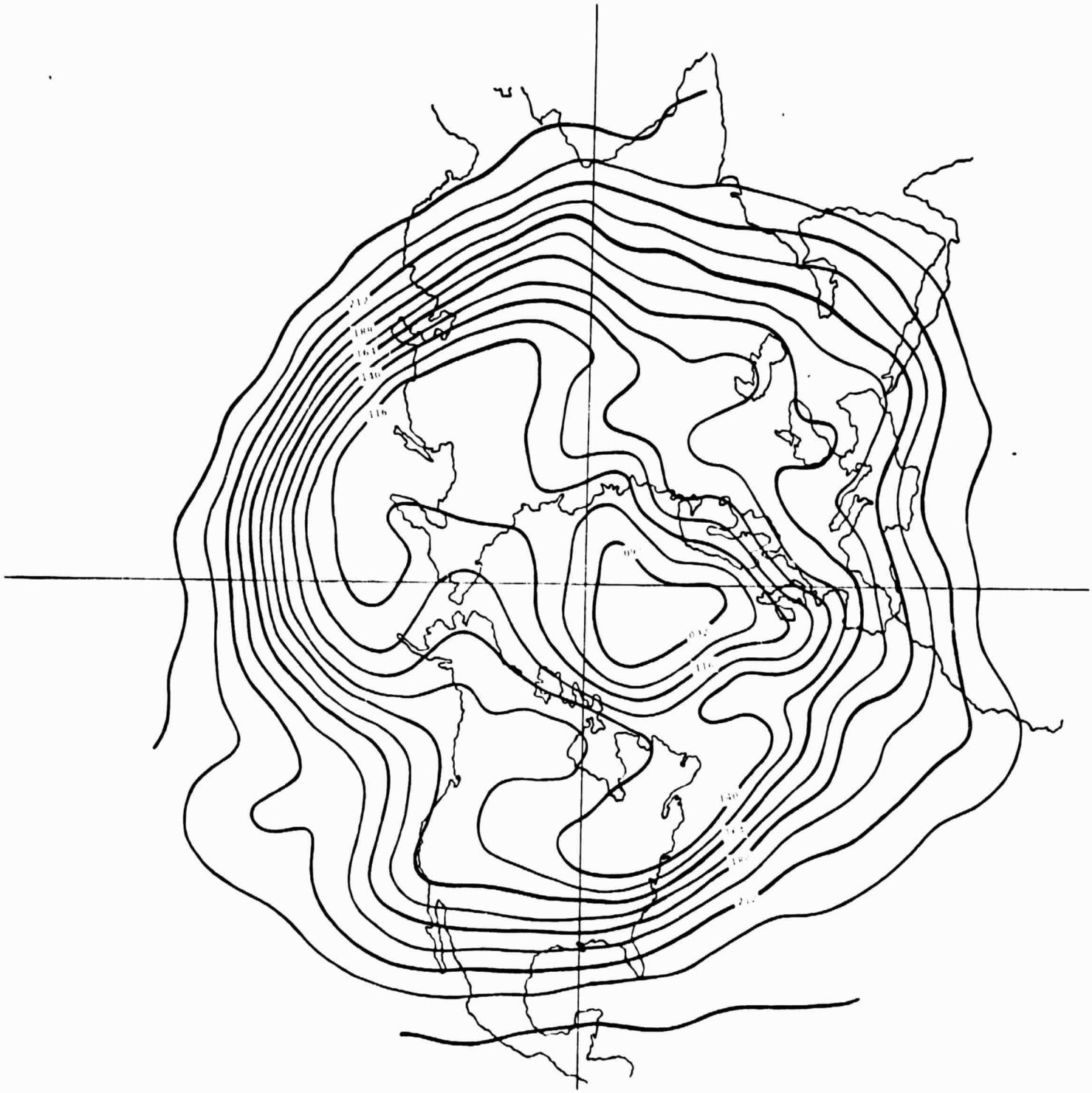

Fig. 1

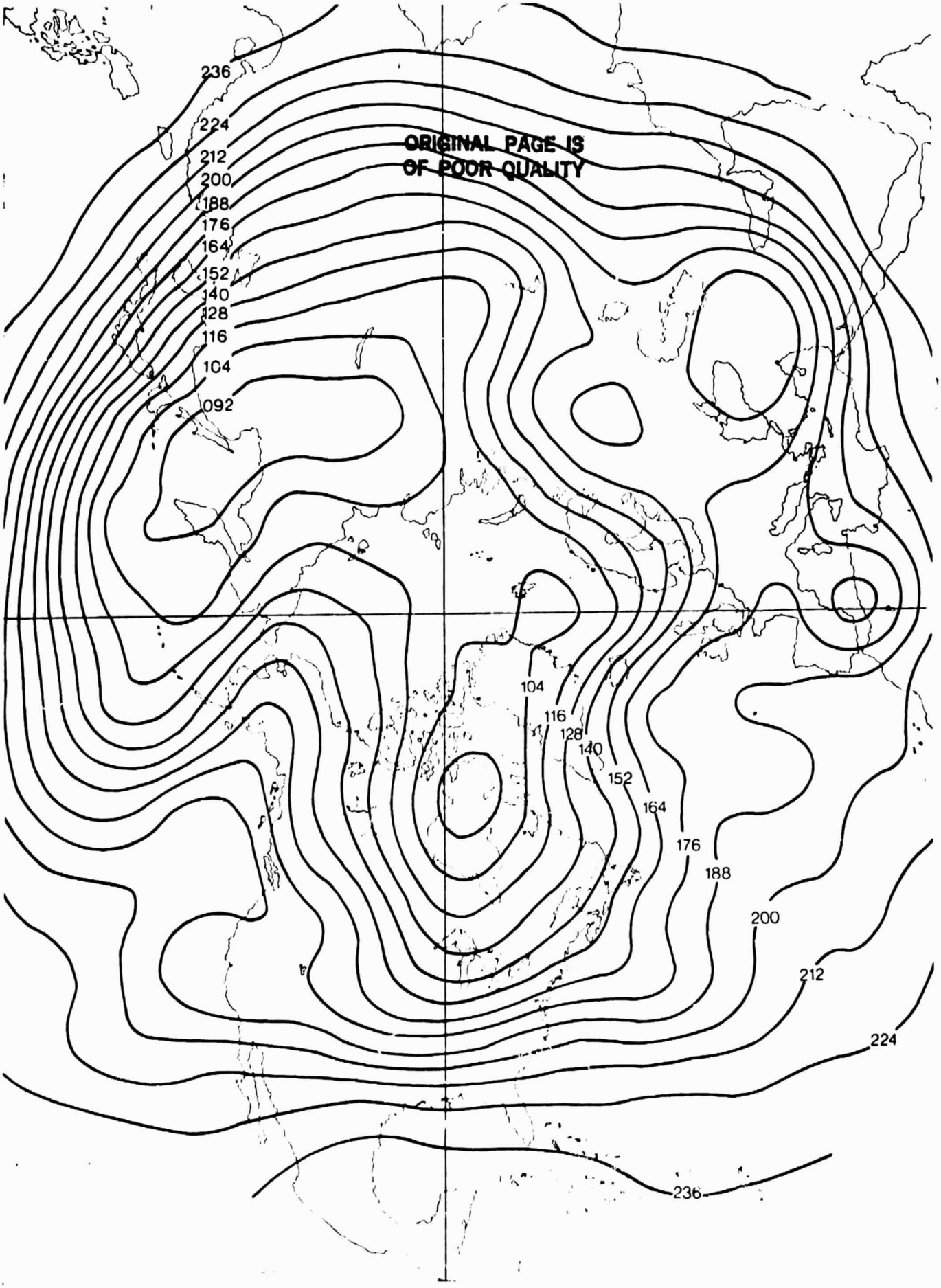
236
224
212
200
188
176
164
152
140
128
116
104
092
ORIGINAL PAGE IS
OF POOR QUALITY
104
116
128
140
152
164
176
188
200
212
224
236

Fig. 2

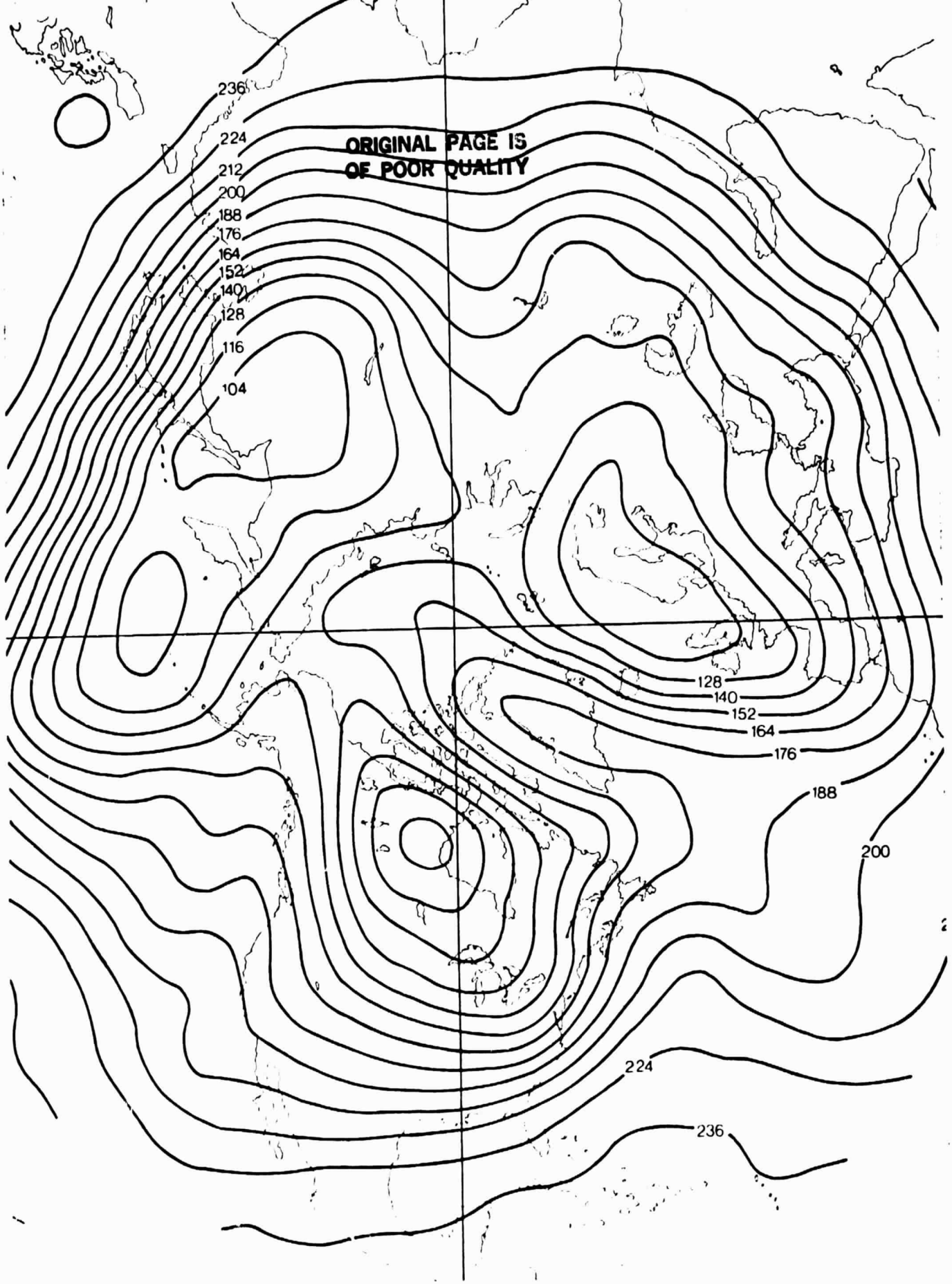
236
224
212
200
188
176
164
152
140
128
116
104
ORIGINAL PAGE IS
OF POOR QUALITY
128
140
152
164
176
188
200
224
236

Fig. 3

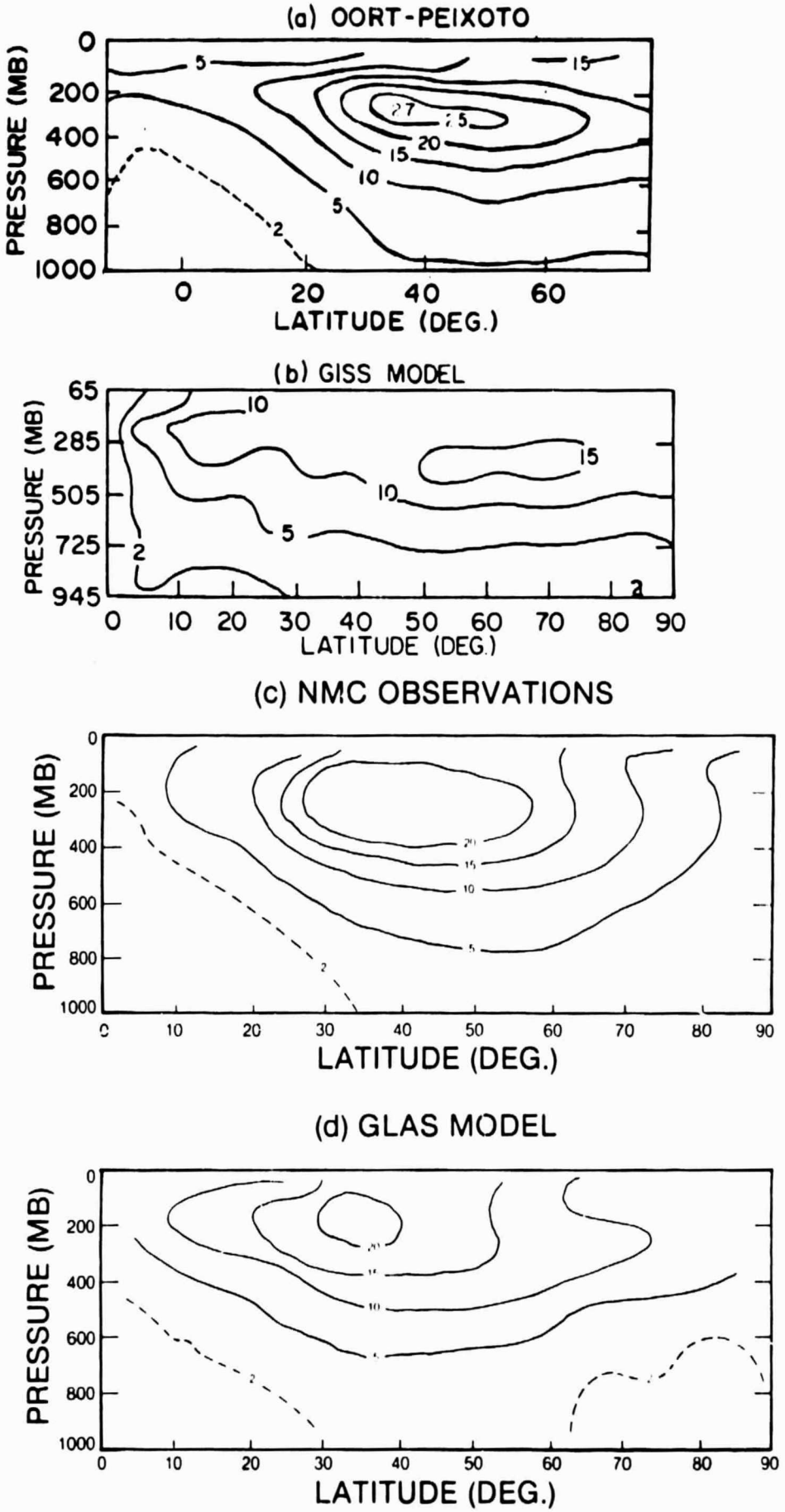
(a) OORT-PEIXOTO
PRESSURE (MB)
0
200
400
600
800
1000
5
15
27
25
20
15
10
5
2
0
20
40
60
LATITUDE (DEG.)
(b) GISS MODEL
PRESSURE (MB)
65
285
505
725
945
10
15
10
5
2
0 10 20 30 40 50 60 70 80 90
LATITUDE (DEG.)
(c) NMC OBSERVATIONS
PRESSURE (MB)
0
200
400
600
800
1000
20
15
10
5
2
0 10 20 30 40 50 60 70 80 90
LATITUDE (DEG.)
(d) GLAS MODEL
PRESSURE (MB)
0
200
400
600
800
1000
0 10 20 30 40 50 60 70 80 90
LATITUDE (DEG.)

Fig. 4

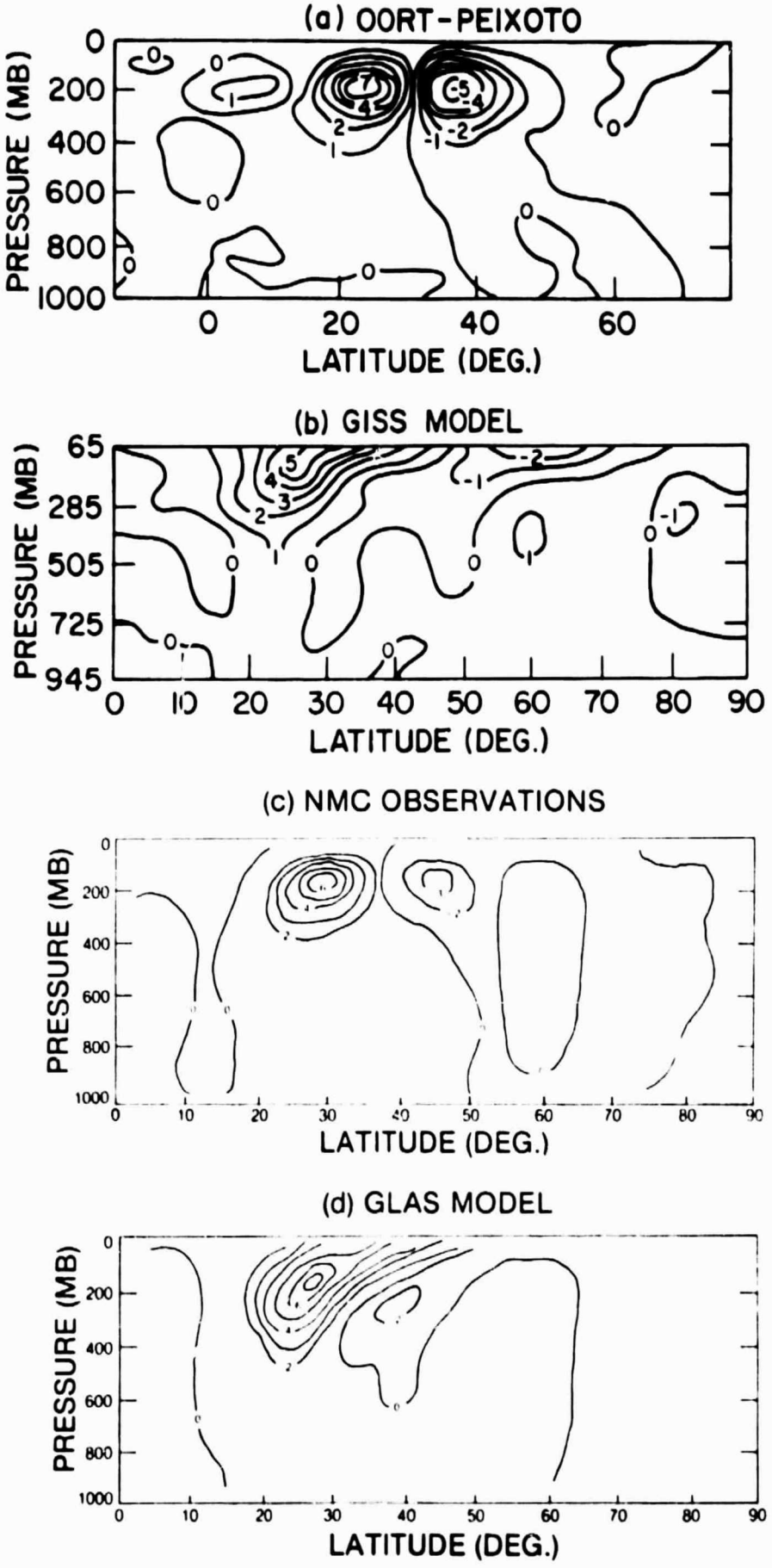
(a) OORT-PEIXOTO
PRESSURE (MB)
0
200
400
600
800
1000
0
20
40
60
LATITUDE (DEG.)
(b) GISS MODEL
PRESSURE (MB)
65
285
505
725
945
0
10
20
30
40
50
60
70
80
90
LATITUDE (DEG.)
(c) NMC OBSERVATIONS
PRESSURE (MB)
LATITUDE (DEG.)
(d) GLAS MODEL
PRESSURE (MB)
LATITUDE (DEG.)

Fig. 5

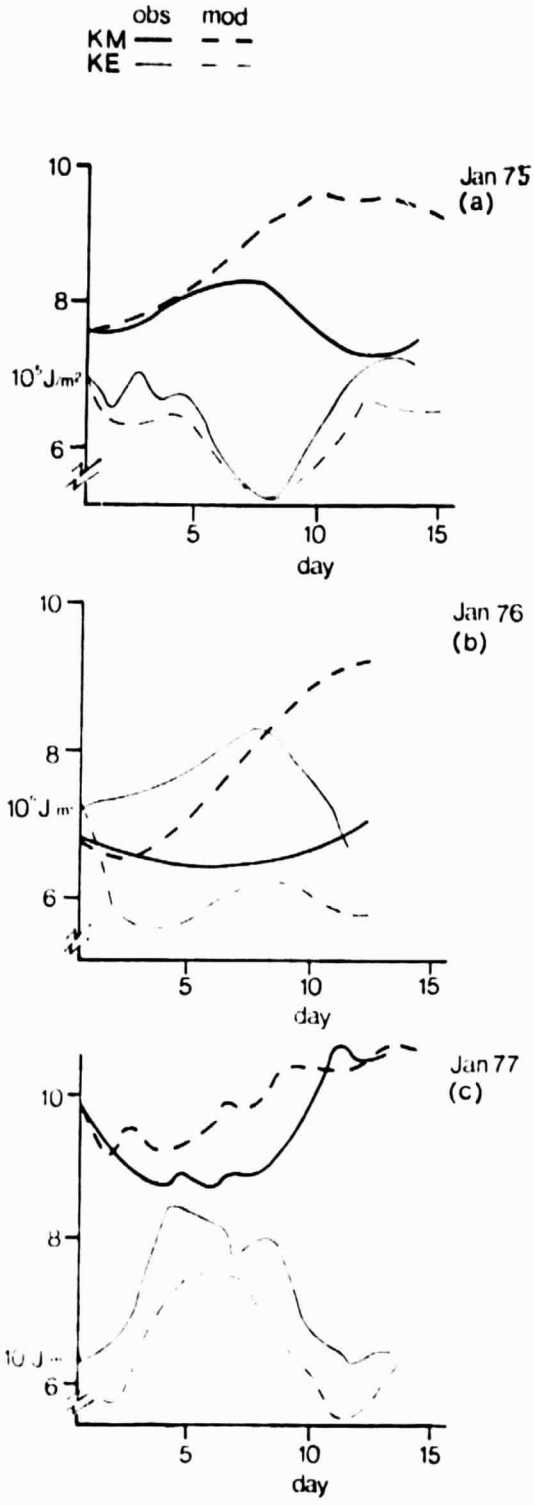
obs
mod
KM
KE
Jan 75
(a)
10
8
6
$10^5$ J/m²
5
10
15
day
Jan 76
(b)
10
8
6
5
10
15
day
Jan 77
(c)
10
8
6
5
10
15
day

Fig. 6

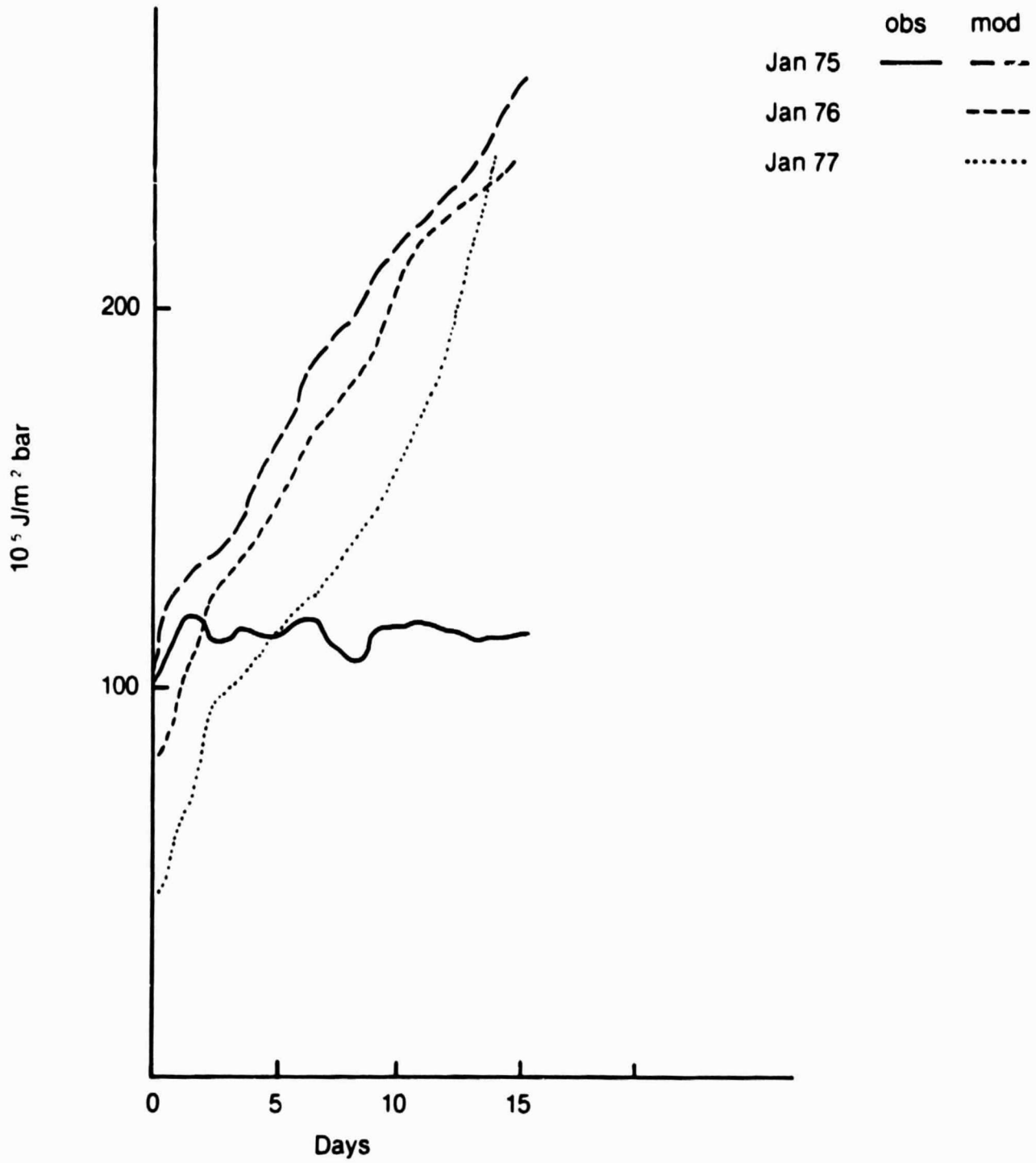


Fig. 7

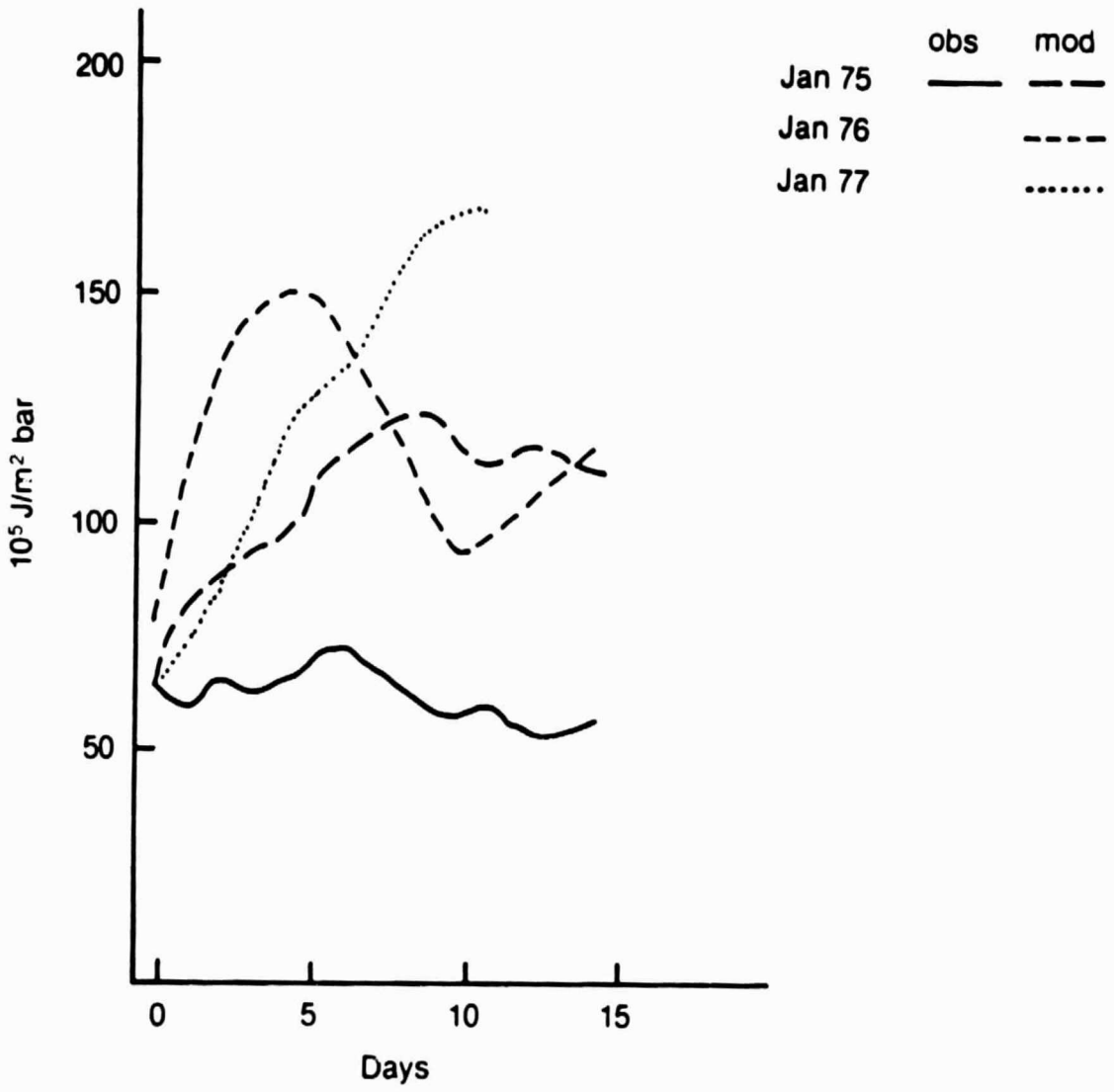
obs
mod
Jan 75
Jan 76
Jan 77
200
150
100
50
$10^5$ J/m$^2$ bar
0
5
10
15
Days

Fig. 8

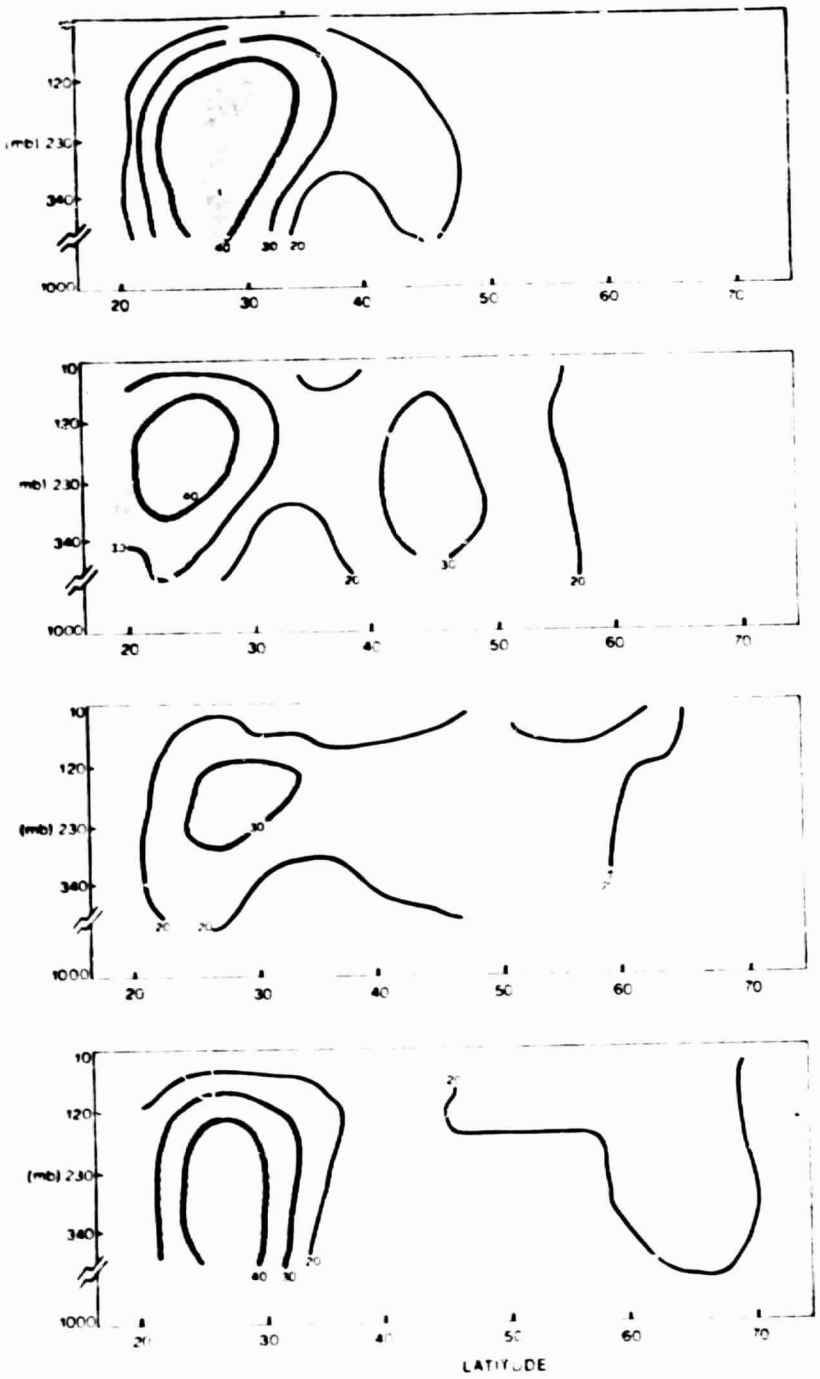


(a)

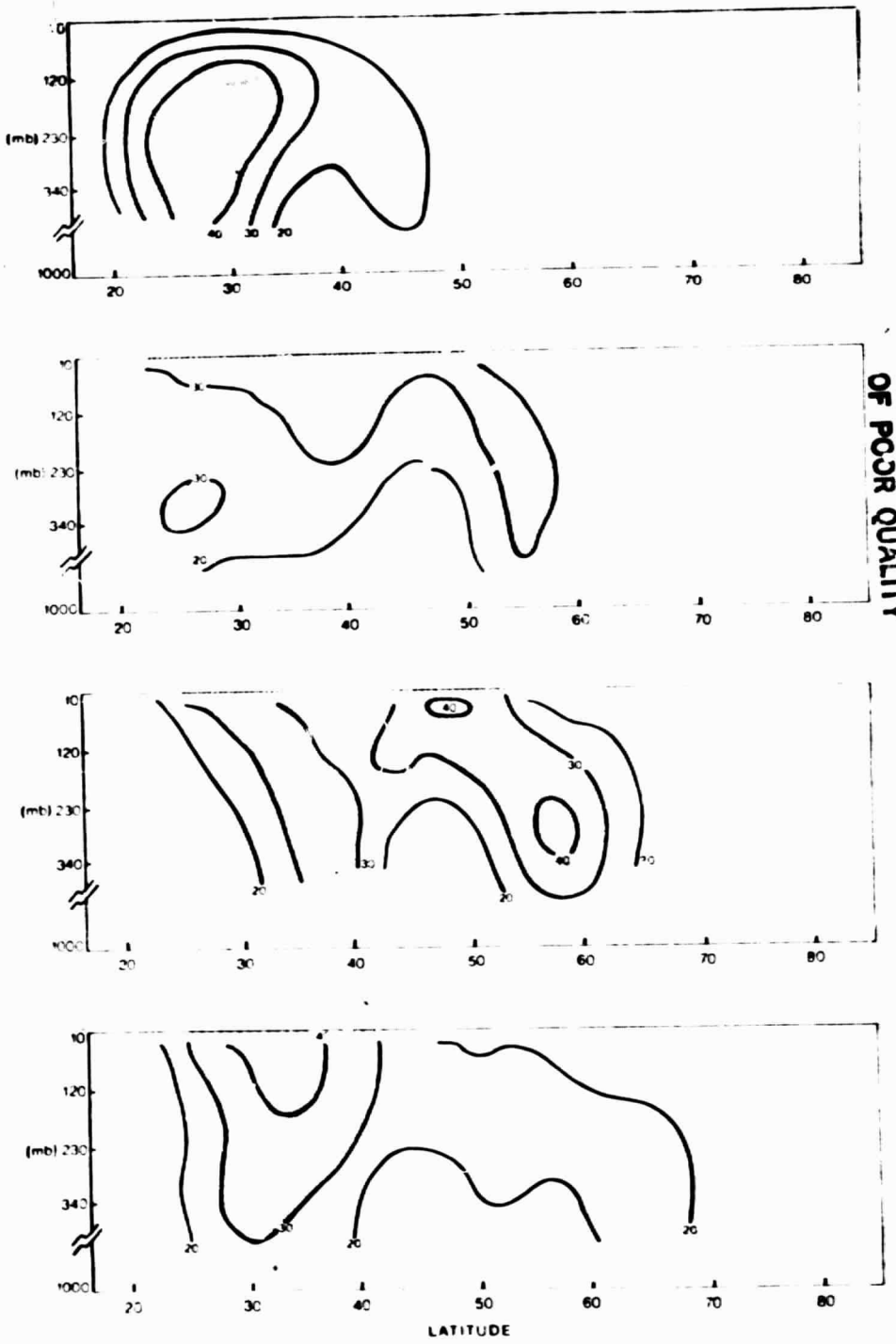


(b)

Fig. 9

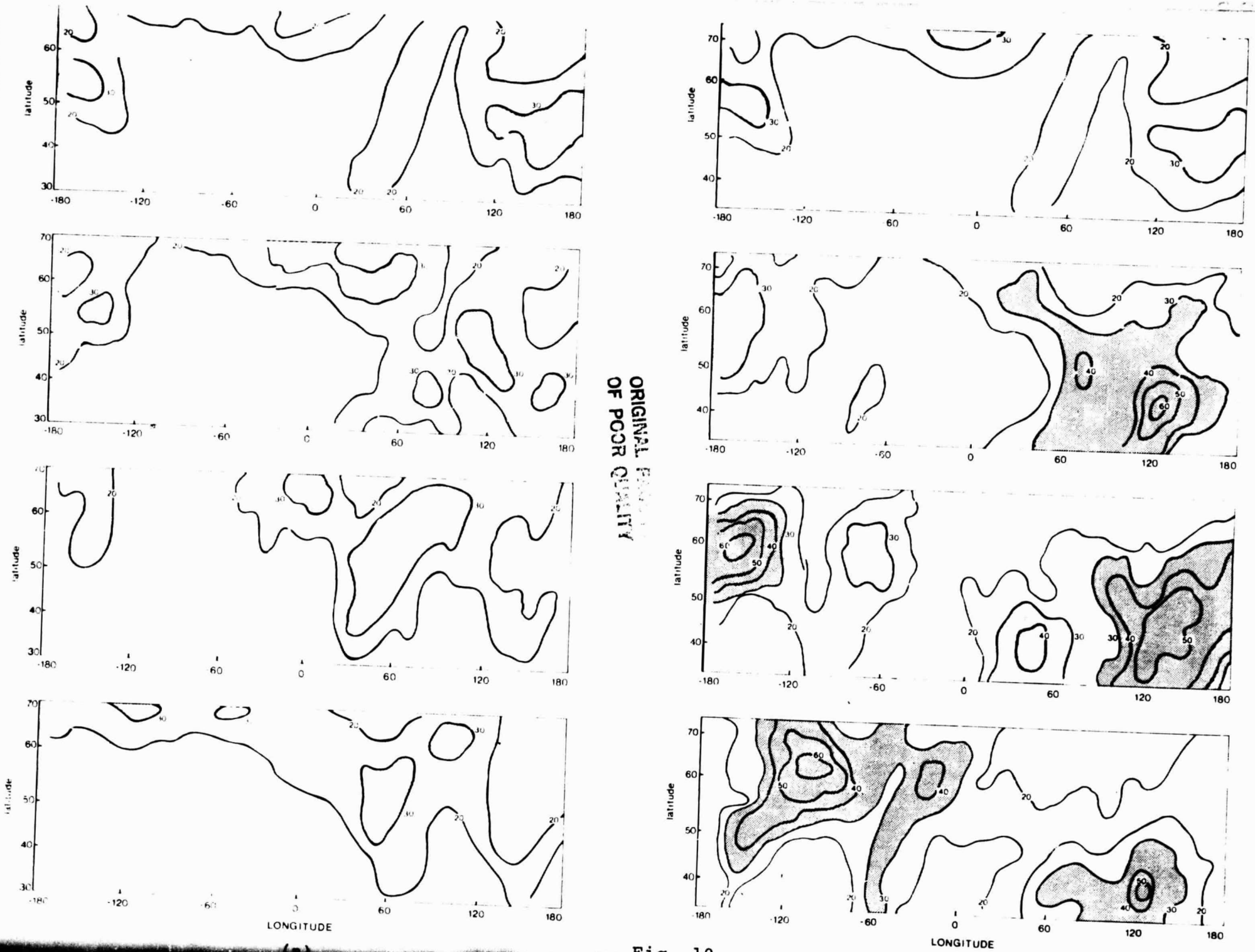




Fig. 10

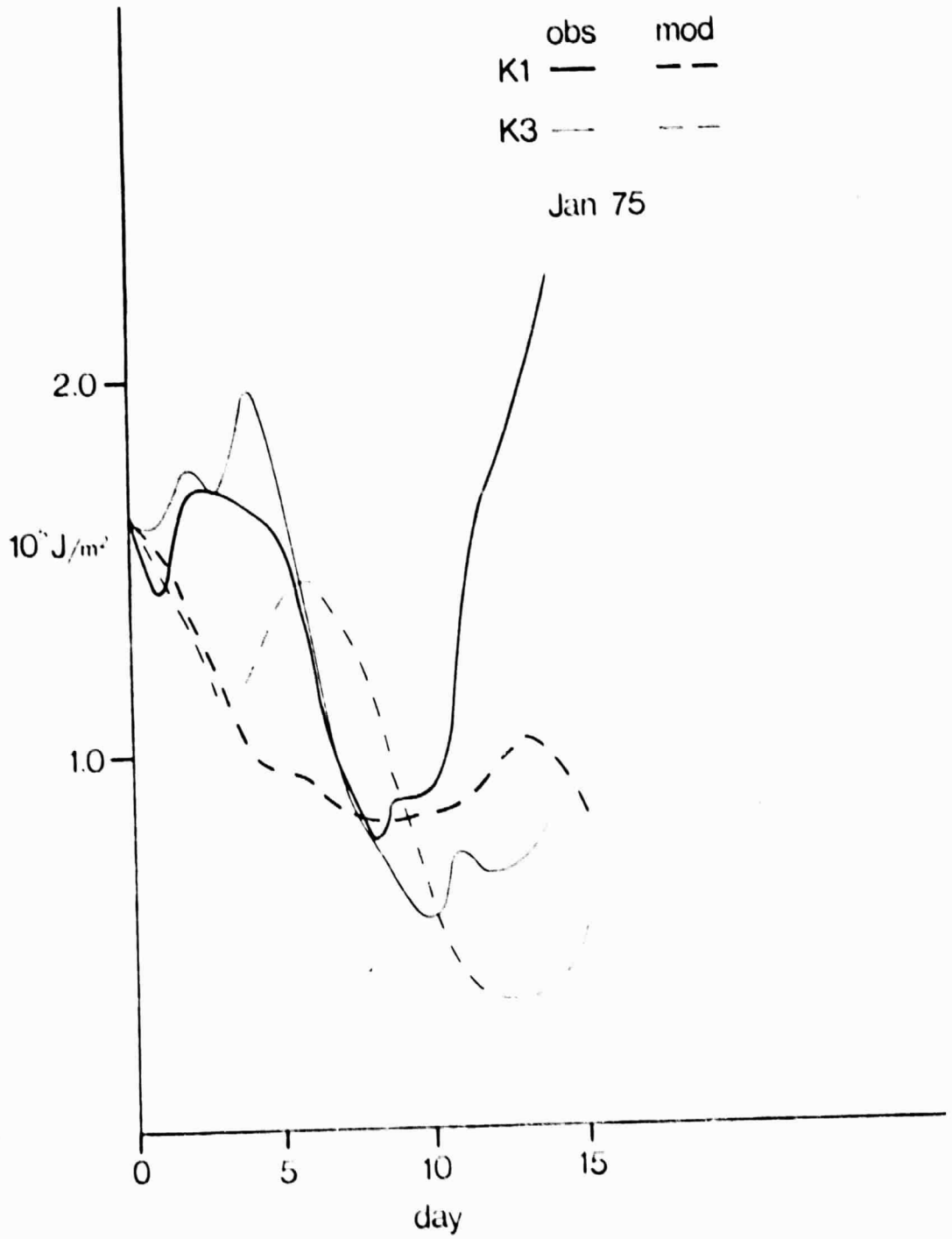


Fig. 11 (a)

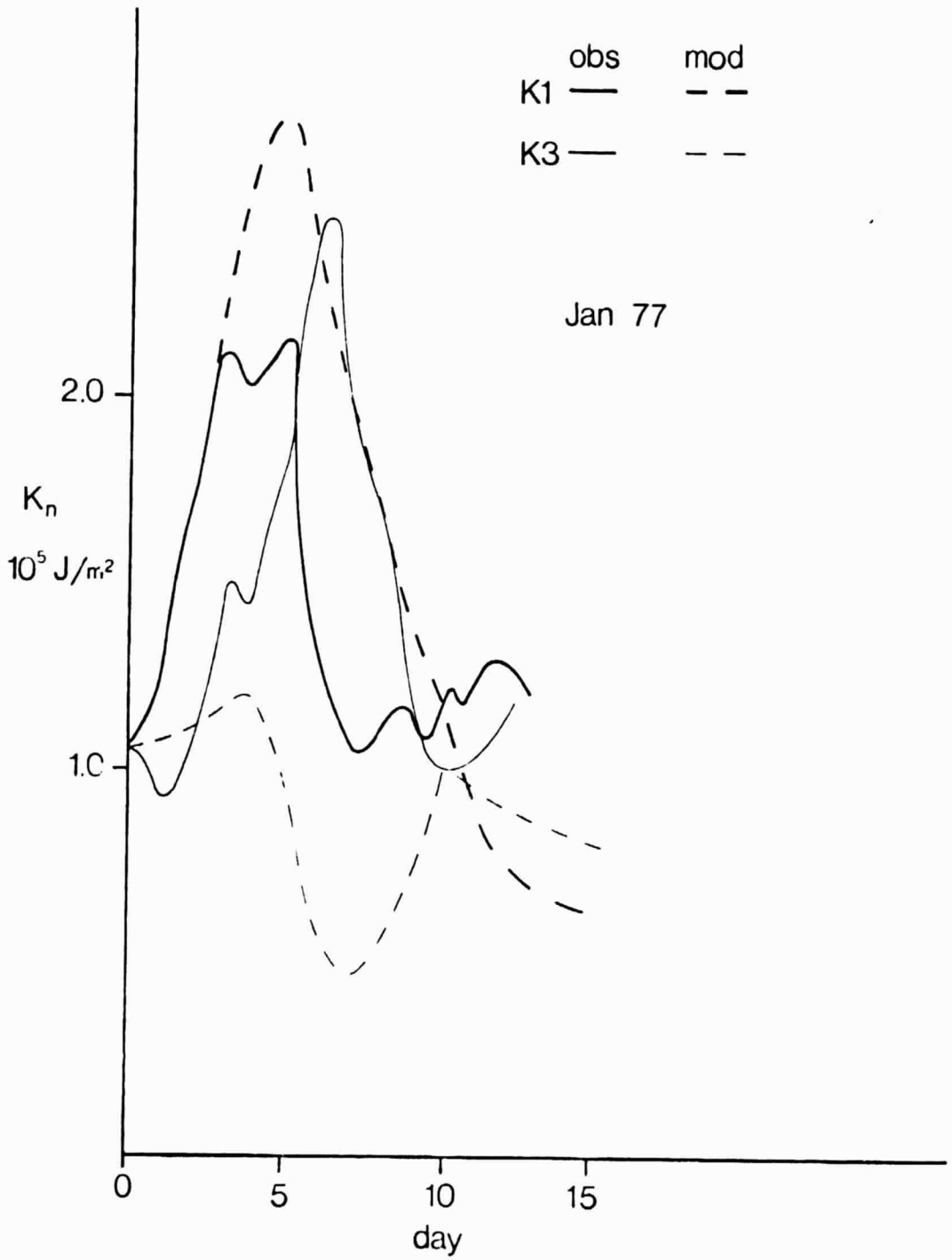


Fig. 11 (b)

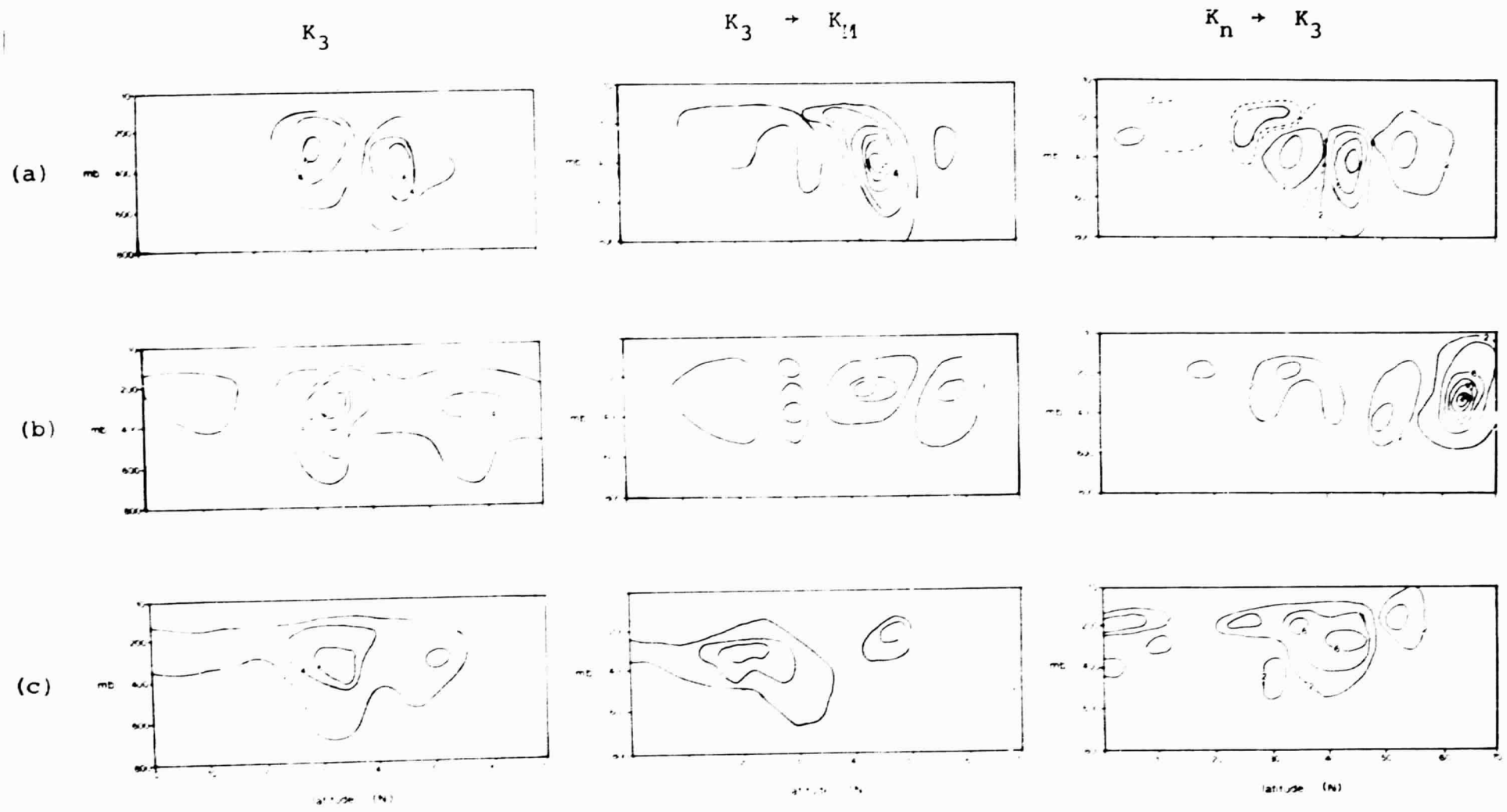


Fig. 12

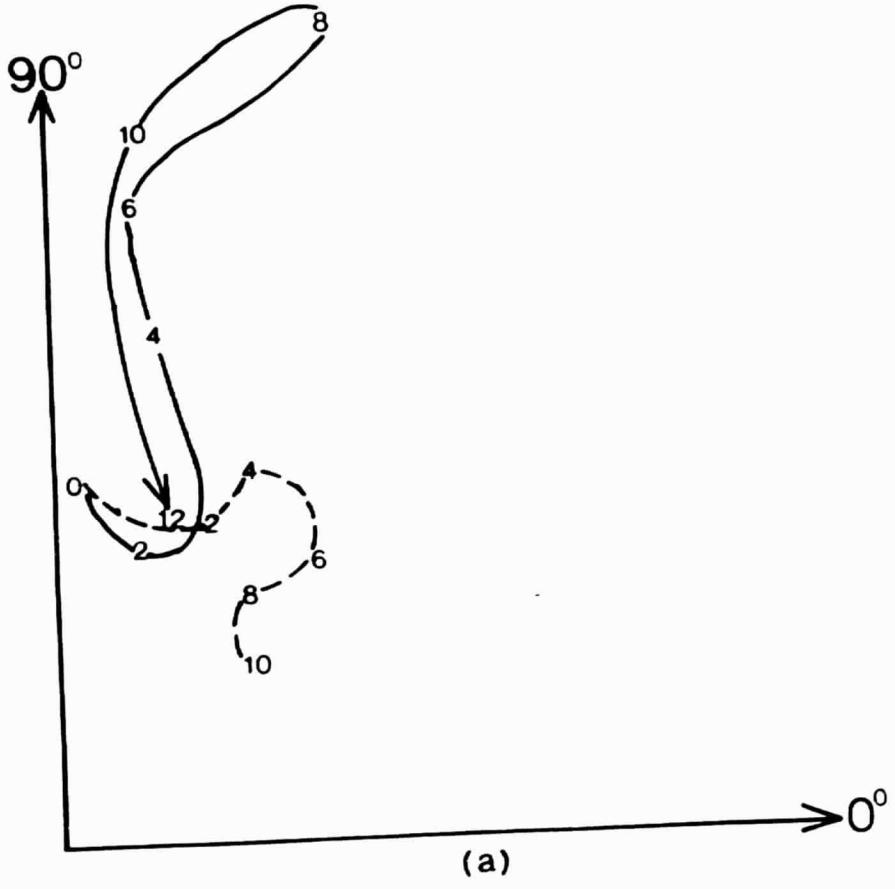


(a)

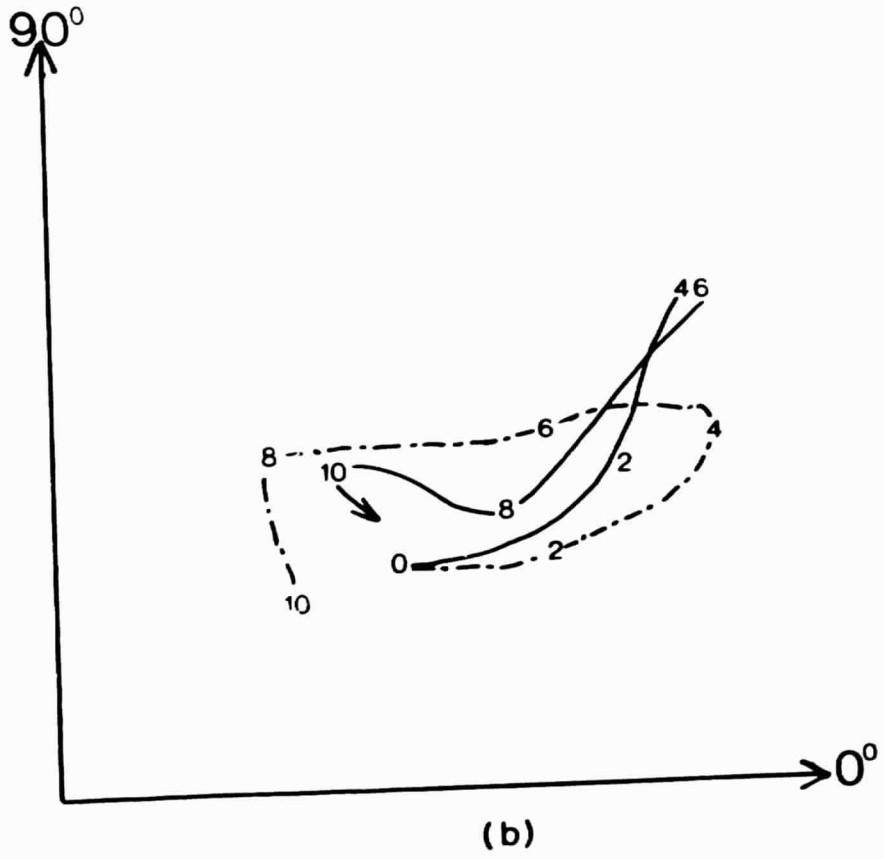


(b)

Fig. 13

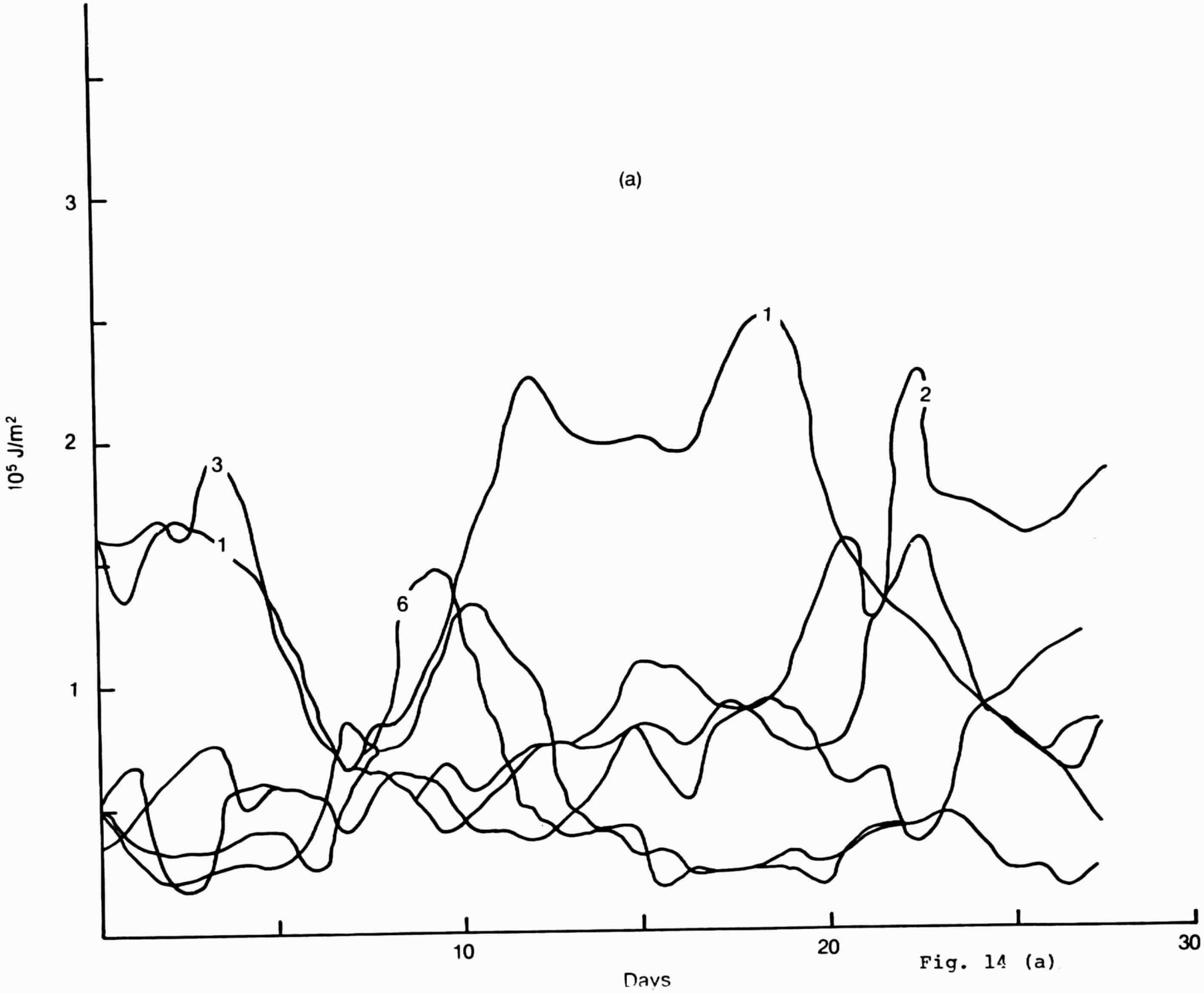


Fig. 14 (a)

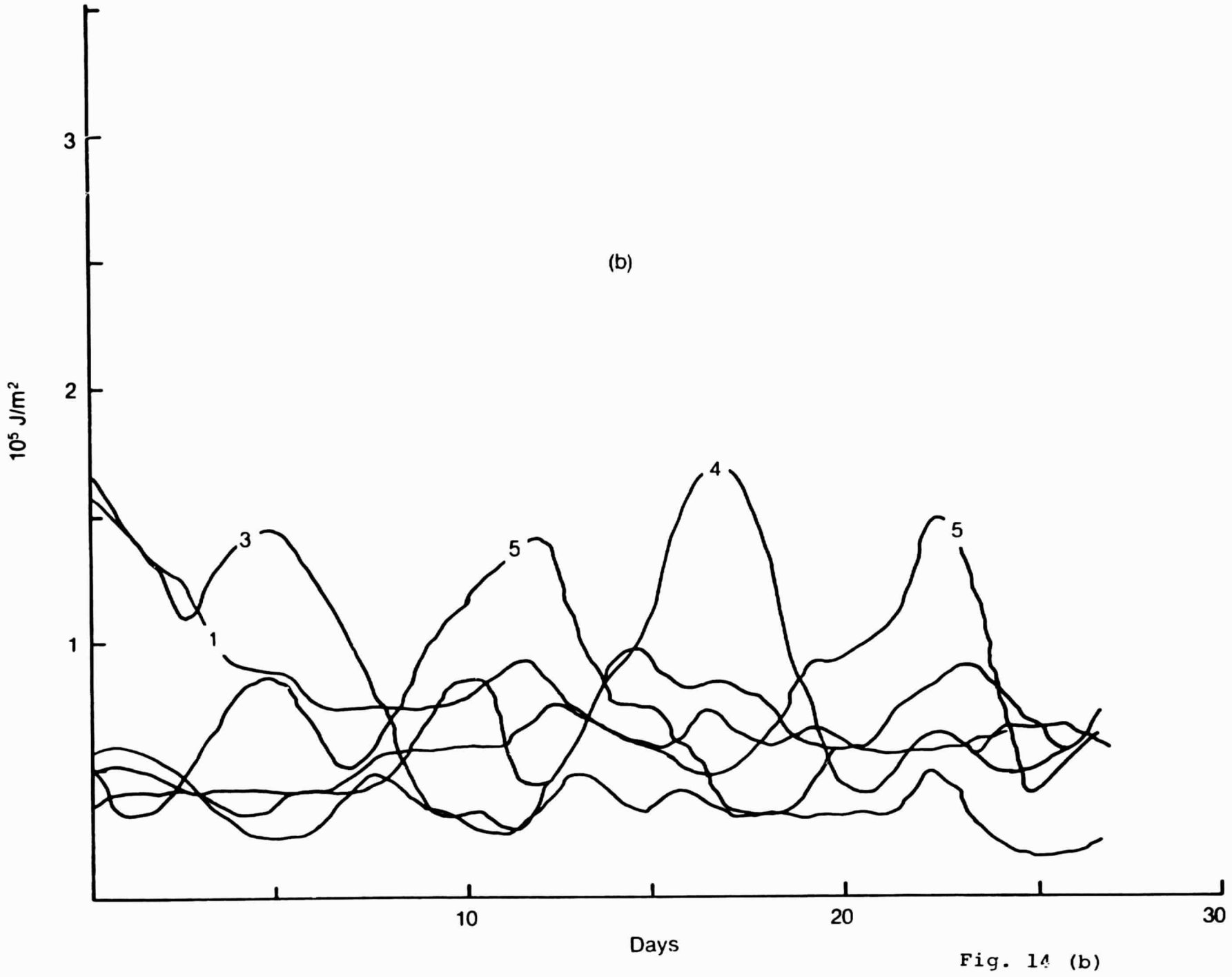


Fig. 14 (b)

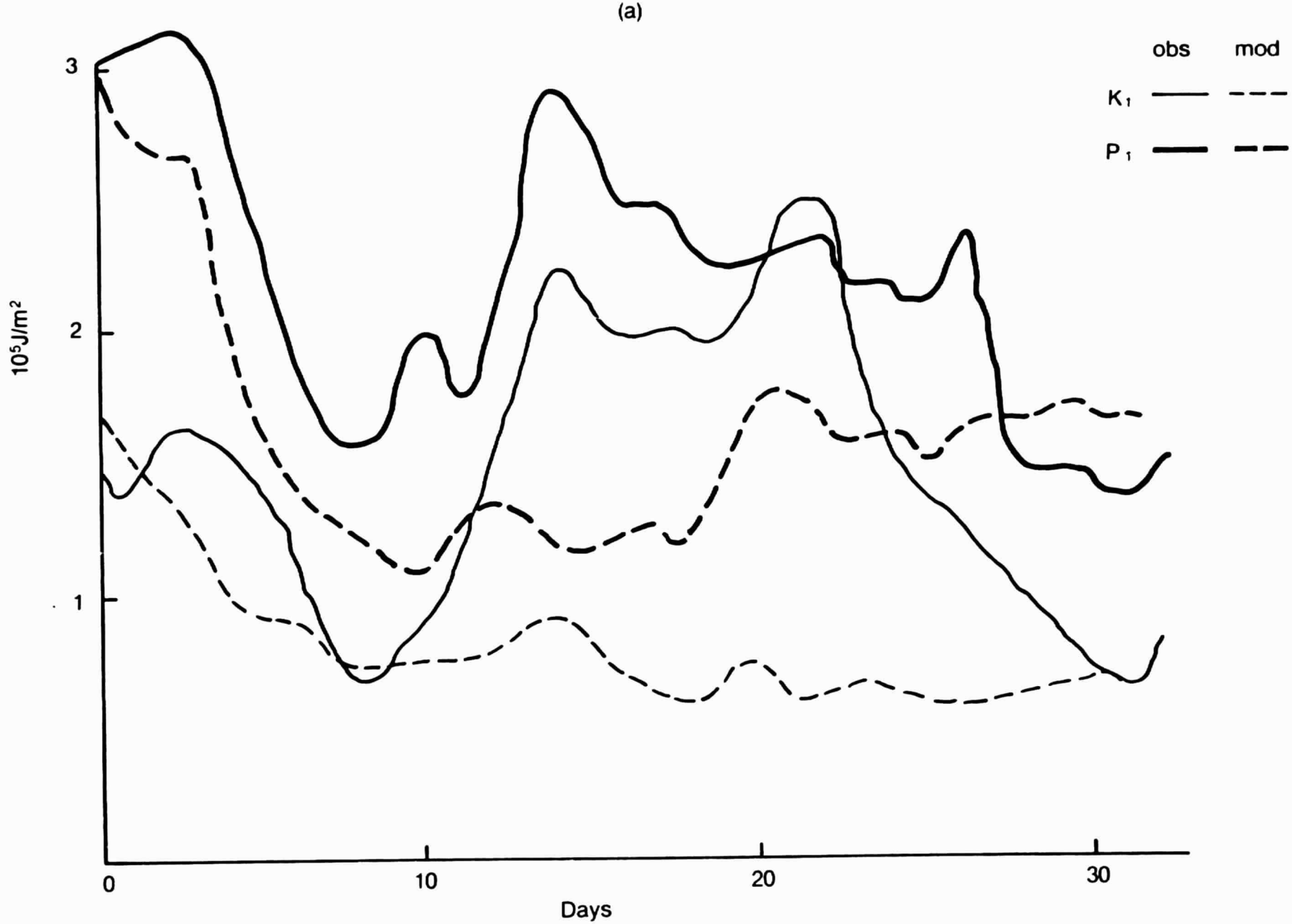


Fig. 15 (a)

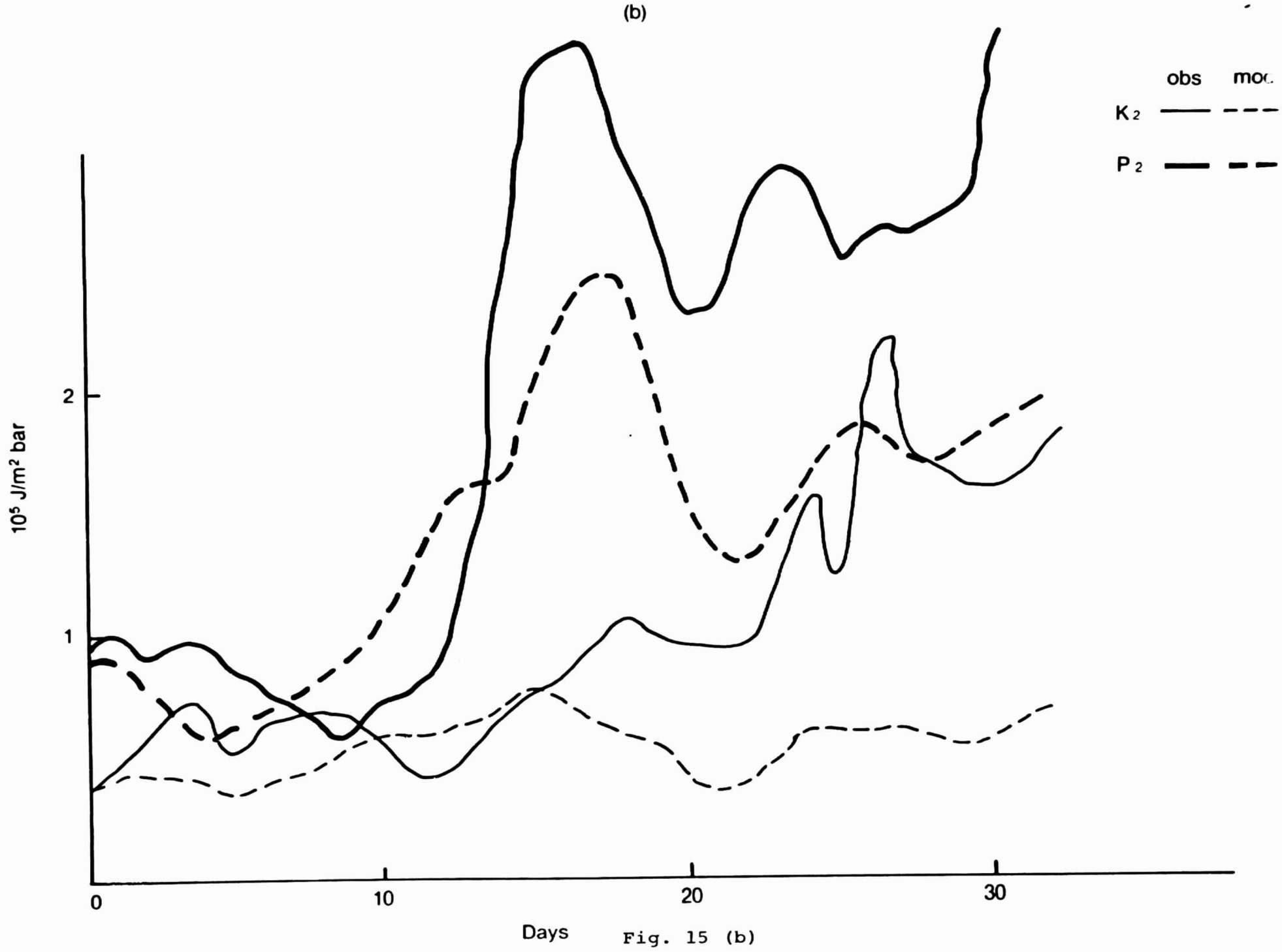


Fig. 15 (b)

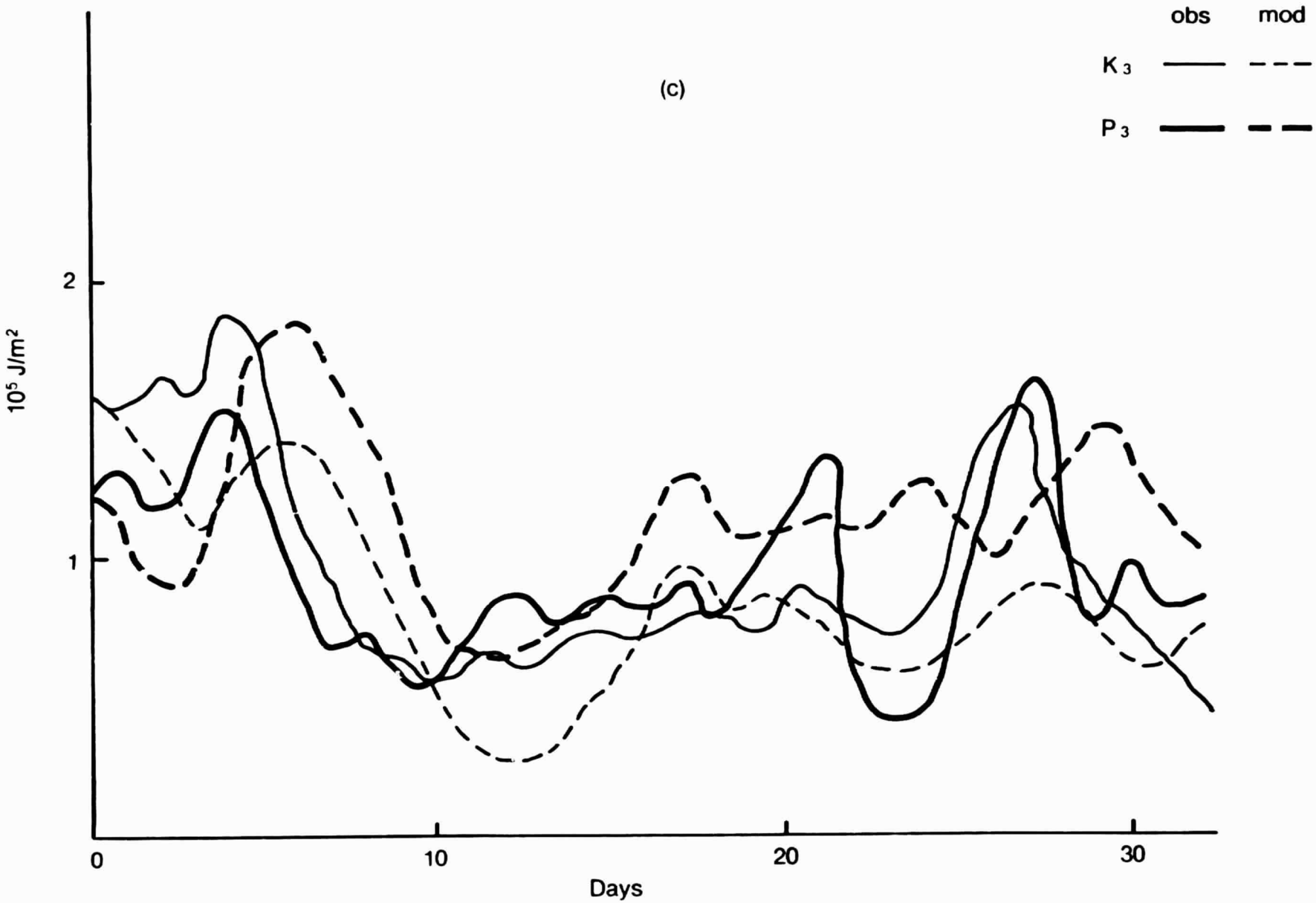


Fig. 15 (c)